Boundary-Layer Meteorology (2020) 177:541–581
https://doi.org/10.1007/s10546-020-00556-3

RESEARCH ARTICLE

Large-Eddy Simulation of the Atmospheric Boundary Layer

Rob Stoll[1] · Jeremy A. Gibbs[2] · Scott T. Salesky[3] · William Anderson[4] · Marc Calaf[1]

Received: 24 March 2020 / Accepted: 21 July 2020 / Published online: 18 August 2020

Abstract
Over the last 50 years the large-eddy simulation (LES) technique has developed into one of the most prominent numerical tools used to study transport processes in the atmospheric boundary layer (ABL). This review examines development of the technique as a tool for ABL research, integration with state-of-the-art scientific computing resources, and some key application areas. Analysis of the published literature indicates that LES research across a broad range of applications accelerated starting around 1990. From that point in time, robust research using LES developed in several different application areas and based on a review of the papers published in this journal, we identify seven major areas of intensive ABL–LES research: convective boundary layers, stable boundary layers, transitional boundary layers, plant canopy flows, urban meteorology and dispersion, surface heterogeneity, and the testing and development of subgrid-scale (SGS) models. We begin with a general overview of LES and then proceed to examine the SGS models developed for use in ABL–LES. After this overview of the technique itself, we review the specific model developments tailored to the identified application areas and the scientific advancements realized using the LES technique in each area. We conclude by examining the computational trends in published ABL–LES research and identify some resource underutilization. Future directions and research needs are identified from a synthesis of the reviewed literature.

✉ Rob Stoll
rstoll@eng.utah.edu

Jeremy A. Gibbs
jeremy.gibbs@noaa.gov

Scott T. Salesky
salesky@ou.edu

William Anderson
wca140030@utdallas.edu

Marc Calaf
marc.calaf@utah.edu

1 Department of Mechanical Engineering, University of Utah, Salt Lake City, UT 84112, USA

2 NOAA/OAR National Severe Storms Laboratory, Norman, OK, USA

3 School of Meteorology, University of Oklahoma, Norman, OK 73072, USA

4 Department of Mechanical Engineering, The University of Texas at Dallas, Richardson, TX, USA

Keywords Convective boundary layer · Large-eddy simulation · Plant canopy · Stable boundary layer · Subgrid-scale model · Urban canopy layer

1 Introduction

A central component of atmospheric boundary layer (ABL) research is the study of turbulent fluxes of mass, momentum, heat, and pollutants (Garratt 1992). These fluxes govern land–atmosphere interactions critical to a wide variety of applications including weather and climate prediction (Teixeira et al. 2008; Holtslag et al. 2013), agricultural water use and productivity (Brutsaert 1982), the dispersion of pollen and spores in natural and agricultural systems (Mahaffee and Stoll 2016), urban air quality and energy use (Pardyjak and Stoll 2017), and many others. Because of their role in a wide range of environmental processes, researchers have developed an array of methods to probe turbulence in the ABL, each with its own strengths and weaknesses (LeMone et al. 2019).

One of the most prominent numerical methods used to examine turbulence in the ABL is the large-eddy simulation (LES) technique. In LES, the conservation equations of mass, momentum, heat, and scalars are filtered with a characteristic spatial filter of width Δ (Lesieur et al. 2005; Sagaut 2006; Wyngaard 2010), which in the ABL with the assumptions of a Boussinesq fluid subject to horizontal Coriolis forces results in

$$\frac{\partial \tilde{u}_i}{\partial x_i} = 0 \tag{1}$$

$$\frac{\partial \tilde{u}_i}{\partial t} + \tilde{u}_j \frac{\partial \tilde{u}_i}{\partial x_j} = -\frac{1}{\rho}\frac{\partial \tilde{p}}{\partial x_i} - f_c \epsilon_{ij3} u_j - \delta_{i3}\frac{\tilde{\theta}_\mathrm{v} - \langle \tilde{\theta}_\mathrm{v} \rangle}{\theta_0} - \frac{\partial \tau_{ij}}{\partial x_j} + F_i \tag{2}$$

$$\frac{\partial \tilde{\theta}}{\partial t} + \tilde{u}_i \frac{\partial \tilde{\theta}}{\partial x_i} = -\frac{\partial q_i}{\partial x_i} + Q \tag{3}$$

where the $\tilde{\ldots}$ indicates a quantity that is filtered with a low-pass convolution filter (Sagaut 2006), u_i is the velocity, with $i = 1$–3 representing the streamwise (u), spanwise (v), and surface normal (w) velocity components, respectively, x_i is the spatial coordinate corresponding to directions of the $\tilde{u}\,(x_i, t)$, $\tilde{v}\,(x_i, t)$, and $\tilde{w}\,(x_i, t)$ velocity components, p is the dynamic pressure, ρ is air density, f_c is the Coriolis frequency at a pre-defined latitude, $\theta(x_i, t)$ represents the potential temperature or a generic scalar concentration for the transport of moisture, pollutants, or other transported scalars, θ_v is the virtual potential temperature, θ_0 is a reference virtual potential temperature, averaging over a region of interest is denoted by angle brackets, $\langle \ldots \rangle_a$, where a, when present, is the dimension over which averaging is performed, Q is a volumetric source or sink of heat or scalar, τ_{ij} and q_i represent the contribution of subfilter-scale (SFS) stress and flux, respectively, and F_i represents a generic body force used to represent the momentum-depleting influence of non-boundary porous or solid objects in the flow (e.g., trees or buildings using a porous flow or immersed boundary method). In Eqs. 2 and 3, viscous effects have been neglected. This is a standard assumption in LES of the ABL where the Reynolds number is typically very large.

The LES technique and its use in the atmospheric sciences has origins in Smagorinsky (1963) and Lilly (1967). Since that time, its use has expanded considerably and it is now one of the dominant numerical techniques used to examine turbulent fluxes in a wide range of atmospheric and engineering applications. This is borne out by examining the percentage of total annual articles published in three representative journals in which LES is a notable component. The considered journals include one focused on ABL research (*Boundary-Layer*

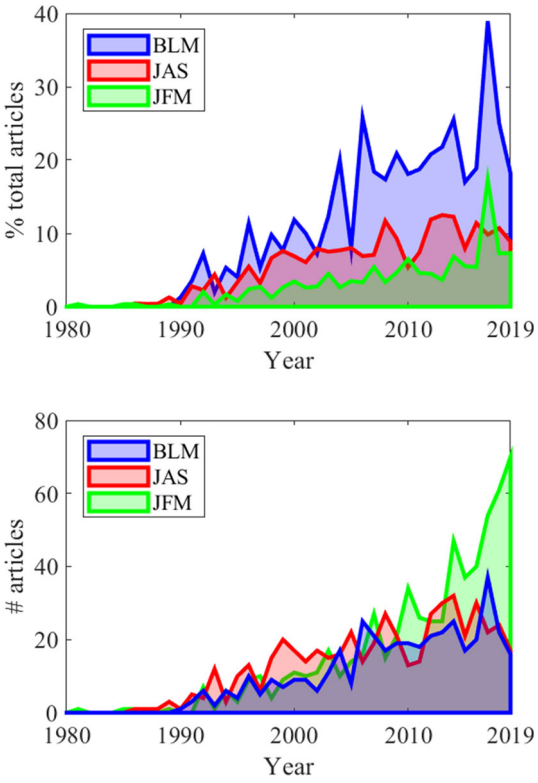

Fig. 1 LES articles published in *BLM* in each year (blue), *JAS* (red), and *JFM* (green) since 1980. The top panel is the percentage of total annual published articles, and the bottom panel is the total number of published articles, in which LES was a prominent component

Meteorology, BLM), one focused on general atmospheric science research (*Journal of the Atmospheric Sciences, JAS*), and one that publishes exemplary research in all classes of fluid mechanics (*Journal of Fluid Mechanics, JFM*). This review focuses on ABL–LES and to that end, *JAS* and *JFM* were chosen to provide context for trends observed in *BLM*, which we use as a proxy for general ABL research due to its relatively specific focus. Articles were included if they referenced LES in their keywords, title, or abstract. This does not mean that all articles are numerical in nature, only that the LES technique plays a prominent role in the presented research.

The most obvious trend shown in Fig. 1 is the upward trajectory in the number of articles mentioning LES in all three journals since 1990. While a definitive reason for the timing of this inflection is difficult to surmise, the early 1990s saw several advances in computational science that likely contributed to the rapid spread of LES. These include the first massively parallel and widely available computing clusters (Castagnera et al. 1994), the standardization of the message passing interface (MPI, Gropp et al. 1996), and the introduction of the Pentium® line of microprocessors (Colwell 2019). A second observation is the clear importance of LES in ABL research. Starting from 2006, almost 20% of all articles published in *BLM* featured LES with a maximum of 39% in 2017. Just as striking is that, although *JFM* and *JAS* both currently publish approximately six times more articles per year than *BLM*, *BLM* publishes a nearly equal amount of LES articles as *JAS* and on the order of half that of *JFM*.

Large-eddy simulation articles published in *BLM* cover a wide range of topics (Fig. 2). The word cloud consists of keywords from all identified LES papers (as described above) with a minimum of four mentions. General keywords that appear in many articles but are

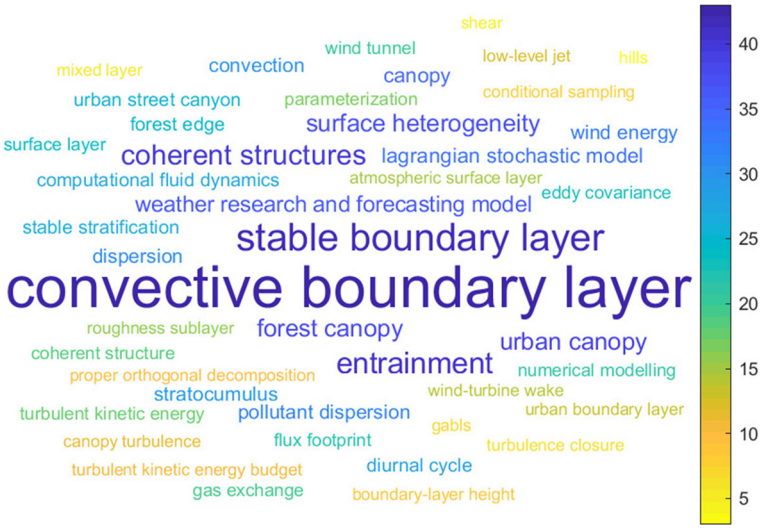

Fig. 2 Word cloud of keywords from LES articles in *BLM*. The colour and relative size of each keyword indicates the number of instances of its usage. Keywords mentioned fewer than four times are excluded

not related to the LES topic of inquiry are excluded for clarity (e.g., atmospheric boundary layer, large-eddy simulation). While the breadth of topics is extensive, a few research areas stand out and these areas have been chosen in this review for detailed analysis. The most prominent is one of the first ABL topics to be explored (Deardorff 1972a), the convective boundary layer (CBL) and its closely related topics (entrainment, mixed layer, convection). A clear second, is research on the stable boundary layer (SBL) and stable stratification. After this, topic areas are still identifiable but the author self-identified topic names become less uniform. The areas we identified include flow in and around plant canopies, dispersion and flow in urban canopies, and heterogeneity and complex terrain. We also find that many articles study the diurnal variation of the ABL and therefore, we explore transitional boundary layers.

Some areas of research are conspicuously missing, e.g., LES of the cloud-topped boundary layer. Performing LES of cloud-topped boundary layers entails modelling challenges related to the representation of cloud microphysics and strong stratification (Yamaguchi and Randall 2012; Mellado 2017) that are somewhat unique. The cloud modelling community has a robust history of simulation intercomparison studies and interested readers are directed to those for detailed descriptions of LES of the cloudy boundary layer (e.g., Stevens et al. 2005; Ackerman et al. 2009). The selected research areas reflect the focus on *BLM* and topics that are prominent in it. Other areas, for example a priori studies of LES SFS models, which have been critical in the development of LES, are not included for brevity. A review of recent developments in cloud-topped boundary layers, a priori studies, and other topics not covered here can be found in LeMone et al. (2019). In addition to the ABL application areas discussed above, we start our review with an examination of the development of the LES technique with an emphasis on the history of SFS model evolution.

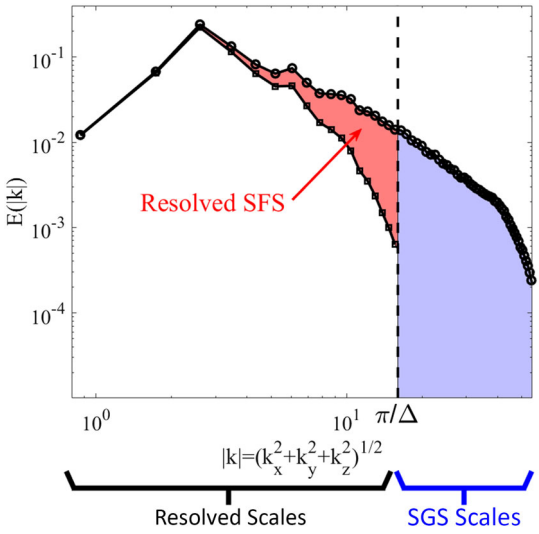

Fig. 3 Illustration of the difference between SFS and SGS using a three-dimensional velocity spectrum obtained from the isotropic turbulence direct numerical simulations of Lu et al. (2008) as an example flow (open circles) and a LES convolution filter with a Gaussian filter kernal (open squares). The red-filled region indicates resolved SFS and the blue-filled region indicates scales that are subgrid

2 LES Technique and SFS Model Development

The LES technique was first introduced in Smagorinsky (1963), expounded upon and formalized by Lilly (1967), and implemented by Deardorff (1970a, 1972a, 1973, 1980). Interestingly, the term "large-eddy simulation" was never used in these seminal works; it was apparently coined in 1973 by W. C. Reynolds at the Center for Turbulence Research, Stanford University (Moin and Homsy 2017), while Leonard (1974) was the first to use it in published form (Lilly 2000). The name is derived from the conceptual underpinnings of the technique, which represents a compromise in balancing physical realizability with computational burden. With LES, a filter is applied to the conservation equations at Δ in order to decompose the flow field into large energy-containing scales and presumably universal small scales. In *physical* LES, the large scales of the flow (i.e., large eddies) are computed explicitly on the numerical mesh, while the effects of the small scales are modelled (Pope 2004). Although strictly numerical approaches are also possible (*numerical* LES), we will focus on applications of *physical* LES to the ABL (see Grinstein et al. 2007 for background and applications of *numerical* LES).

Before continuing, it is important in this context to distinguish between SFS and subgrid-scale (SGS), despite their colloquial conflation. The latter refers to scales that fall below the grid spacing increment and is often used when the numerical grid spacing acts as the filter width in the LES conservation equations, while the former is meant to describe motions whose scales fall below the width of any explicit filter operation. In other words, SGS motions are always unresolved on the computational mesh, while SFS motions may be partially resolved (Fig. 3). Please note that the presented data are used to demonstrate conceptual aspects of filtering and spectral density; ABL turbulence is additionally affected by land-surface normal heterogeneity.

When a filter is applied to the conservation equations, the terms $\widetilde{u_i u_j}$ and $\widetilde{u_i \theta}$ appear in the resulting expressions for momentum and heat/scalars, respectively. These terms are problematic because they represent the filtered product of two non-filtered variables. One does not have knowledge of these variables and thus the terms cannot be solved a priori. Leonard (1974) decomposed and filtered the nonlinear term in the momentum equation to

obtain $\tau_{ij} = L_{ij}+C_{ij}+R_{ij} = \widetilde{u_i u_j} - \widetilde{u}_i\widetilde{u}_j$. Here, $C_{ij} = \widetilde{\widetilde{u}_i u'_j} + \widetilde{\widetilde{u}_j u'_i}$ describes the interaction between resolved and SFSs, $R_{ij} = \widetilde{u'_i u'_j}$ is the SFS "Reynolds" stress, $L_{ij} = \widetilde{\widetilde{u}_i \widetilde{u}_j} - \widetilde{u}_i\widetilde{u}_j$ is the so-called Leonard stress, which describes the interaction among the smallest resolved scales, and the prime ($'$) denotes deviation from the filtered value. If the filter is a Reynolds operator, then C_{ij} and L_{ij} disappear and $\tau_{ij} = \widetilde{u'_i u'_j}$. A similar procedure is applied for scalars.

Substituting these expressions into the filtered form of the conservation equations yields Eqs. 2 and 3, respectively. However, the SFS stress τ_{ij} and SFS flux q_i are unknown quantities and thus the equations are not closed (the so-called turbulence "closure problem"). The goal of LES is often to generate realistic statistical properties of a considered turbulent flow. To that end, it is a necessary, but not sufficient, condition for an SFS model to provide the correct distributions of mean energy dissipation and stress in order to properly capture flow statistics (Meneveau and Katz 2000). Accordingly, a primary challenge in LES is modelling τ_{ij} and q_i. Much of the early work developing the LES technique focused on these two terms, but it must be recognized that the development and performance of LES SFS models cannot be disentangled from the numerical representation and solution methodology used for Eqs. 1–3. The type of filter used to separate resolved and SFS (Geurts 2003; Wyngaard 2010), the chosen spatial discretization scheme (see Giacomini and Giometto 2020, for a review of techniques), and the chosen time integration scheme (Gibbs and Fedorovich 2014b), all have significant impacts on the representation of turbulence and the effective resolution of a given numerical code (Moeng and Wyngaard 1988; Gibbs and Fedorovich 2014a). The subject of numerical discretization is a wide ranging one that has a critical role in LES. In this section we give a brief overview of the historical LES technique and SFS model development, with a focus on the physical aspects. For more details on the numerical aspects, see the aforementioned references.

2.1 Eddy-Viscosity Models

Eddy-viscosity (EV) models are the most widely used class of SFS models and are mathematically analogous to the molecular properties of Newtonian fluids. For a constant-property Newtonian fluid, the stress tensor is linearly related to the mean shear through the molecular viscosity of the fluid (Pope 2000). Similarly, EV models assume that the deviatoric part of the Reynolds stress is linearly related to the mean rate-of-strain of a flow through an eddy viscosity

$$\tau_{ij} = -2\nu_T \widetilde{S}_{ij}, \tag{4}$$

$$q_i = -\nu_\theta \frac{\partial \widetilde{\theta}}{\partial x_i}, \tag{5}$$

where ν_T is the eddy viscosity, $\widetilde{S}_{ij} = 0.5\left(\partial\widetilde{u}_i/\partial x_j + \partial\widetilde{u}_j/\partial x_i\right)$ is the filtered strain rate tensor, and ν_θ is the eddy diffusivity.

Examination of even basic turbulent flows has shown that there is no general physical validity to this assumption (Pope 2000). Additionally, EV models extract energy from the simulation's resolved scales, mimicking the average energy transfer in the turbulent cascade, making them purely dissipative and thus they only represent the statistically averaged flow of energy and not the combined instantaneous forward scatter and backscatter observed over large portions of the flow in, e.g., direct numerical simulation (DNS) of channel flow (Piomelli

et al. 1991). Despite these drawbacks, the EV model has proven to be a reasonable approach across a range of flow scenarios.

Smagorinsky (1963) was the first to introduce an EV model in an attempt to parametrize the effects of three-dimensional small-scale motions in simulations of quasi-two-dimensional synoptic-scale atmospheric circulation. The chosen EV related local variables to flow features at a length scale equal to the numerical grid spacing (Métais 1998). The Smagorinsky model was based on work in von Neumann's group at Princeton, in which one-dimensional acoustic shocks were smoothed through the use of an artificial viscosity that was proportional to the local gradient of the flow field and the square of the spacing between data points (Lilly 2000). Although Smagorinsky's model is overly dissipative of large-scale atmospheric motions, it remains popular. More importantly, it served as a catalyst for future development of the LES technique and SFS models. Smagorinsky (1963) proposed the following model, which is based on the mixing-length theory of Prandtl (1925),

$$\tau_{ij} = -2(C_S\Delta)^2|\widetilde{S}|\widetilde{S}_{ij}, \tag{6}$$

where $\Delta = (\Delta_x\Delta_y\Delta_z)^{\frac{1}{3}}$ is a length scale based on the grid-spacing increments in each direction, C_S is a constant, and $|\widetilde{S}| = \sqrt{2\widetilde{S}_{ij}\widetilde{S}_{ij}}$ can be considered as a representative velocity scale for transport at the SFS. Lilly (1967) was the first to derive a filter-dependent, grid-increment-independent expression for C_S. It was shown in op. cit. that $C_S \approx 0.17$ for a spectral cut-off filter under the assumption of Kolmogorov turbulence (Kolmogorov et al. 1991, K-41). These combined efforts explain why Eq. 6 is often referred to as the Smagorinsky–Lilly model.

Deardorff (1970a) first implemented the Smagorinsky–Lilly model in a numerical simulation of plane Poiseuille flow to study turbulence properties at large Reynolds numbers. The modest numerical mesh of $24 \times 14 \times 20$ points was a limitation of memory availability in the CDC 6600 Supercomputer at the National Center for Atmospheric Research. Deardorff tested several values of C_S and found that Lilly's value of 0.17 resulted in excessively damped small-scale motions and subsequently settled on $C_S = 0.10$. Results, as compared with laboratory measurements, were deemed "good to marginal". In follow-up studies using larger numerical grids of up to $40 \times 40 \times 20$ points, Deardorff (1971, 1972a) reported that C_S should be changed to 0.21 (0.13) for unstably (neutrally) stratified flows. The modification was justified by noting that the large-scale mean flow derived from, e.g. a constant pressure gradient, should be removed from the computation of the SGS eddy coefficient. Despite the additional information gleaned from the adjustment to C_S, Deardorff noted the limitations of the Smagorinsky–Lilly model in the presence of stably stratified regions.

Deardorff (1980, D80) used an alternative form for the EV as an approach to improving the representation of stratification without resorting to solving prognostic equations for τ_{ij}. The EV was taken as $\nu_T = C_1\ell\sqrt{E}$, where $C_1 = 0.1$ and $\ell = \Delta(\partial\tilde{b}/\partial x_3 \leq 0)$, $\min\left[\Delta, 0.5\sqrt{E}/N\right](\partial\tilde{b}/\partial x_3 > 0)$ is the turbulence length scale, in which b is buoyancy and N is the Brunt–Väisälä frequency. The SGS kinetic energy E (used in the representative velocity scale) was found using the following parametrized transport equation,

$$\frac{\partial E}{\partial t} = -\frac{\partial\tilde{u}_j E}{\partial x_j} + 2\nu_T\widetilde{S}_{ij}\widetilde{S}_{ij} - \nu_\theta\frac{\partial\tilde{b}}{\partial z} + \frac{\partial}{\partial x_j}2\nu_T\frac{\partial E}{\partial x_j} - \epsilon. \tag{7}$$

The eddy diffusivity and SGS turbulence kinetic energy (TKE) dissipation were modelled, respectively, as

$$\nu_\theta = \left(1 + 2\frac{\ell}{\Delta}\right)\nu_T \quad \text{and} \quad \epsilon = C_e \frac{E^{3/2}}{\ell},$$

where $C_e = \xi_c\,(0.19 + 0.51\ell/\Delta)$ and ξ_c is an optional wall-correction function. The modelled dissipation rate is included to ensure that the mean energy transfer from the resolved scales is balanced in accordance with K-41. While the model is commonly credited to Deardorff, it is similar to one proposed by Schumann (1975) for the isotropic part of a two-part EV model. In fact, Sullivan et al. (1994) proposed a two-part EV model based, in part, on Schumann (1975) and D80 that added mean-shear contributions to the SGS TKE transport equation to improve results near the lower boundary. The D80 model also served as the SGS model in the first pseudo-spectral LES of the ABL (Moeng 1984) and models based on D80 remain popular due to the ability to include SGS transport or energy drain effects as extra parameters in the SGS kinetic energy transport equation. Recently, Gibbs and Fedorovich (2016, GF16) revisited the D80 model and proposed removing the stability-dependent length scale and near-wall enhancement of dissipation if the numerical grid spacing is adequately fine, and introduced a new stability-dependent formulation for ν_θ based on the Richardson number (Ri). The GF16 model better captures near-surface predictions of TKE, stability, and sensible heat flux.

2.2 Alternatives to Eddy-Viscosity Models

Additional methods were motivated by the EV approach pioneered by Smagorinsky. To address deficiencies in early applications of Eq. 6, Deardorff (1973) introduced a second-order model that required closure of the SFS transport equations. The pressure–velocity correlations were ignored while the triple correlation, pressure–strain correlation, and dissipation were modelled as functions of SGS kinetic energy E (which was taken as the square of the relevant velocity scale). While results using the new transport model indicated better representation of fluxes than those predicted by the Smagorinsky–Lilly model, the simulations were 2.5 times more expensive computationally and the model was still subject to the limitations of the EV closure paradigm.

Another set of alternative models use the idea of scale similarity, which assumes that the statistical structure of tensors constructed on the basis of the SFSs is similar to that of the equivalent tensors evaluated using the smallest resolved scales. The idea (loosely motivated by Leonard 1974) is that the unresolved scales and smallest resolved scales have a common history through interactions with the largest resolved scales, and that some structures appear in all three bands leading to strong correlations among each level of decomposition. Bardina et al. (1980) proposed the first scale-similarity model, which was later generalized by Liu et al. (1994). Scale-similarity models were quite computationally expensive due to the use of multiple explicit filtering operations. This limitation motivated the development of nonlinear models, which approximate $\widetilde{u}_i$ by a Taylor series expansion around the "true" mean at a point. This procedure is far less computationally expensive since no additional explicit filtering operations are required.

Although similarity and nonlinear models exhibit a high level of correlation in a priori tests with measured values of τ_{ij}, they underestimate the average dissipation and are numerically unstable. As a result, they are combined with an EV model to provide the proper level

of dissipation. In ABL research, mixed models have been implemented using the explicit filtering and reconstruction method described in Chow et al. (2005) and Mirocha et al. (2010).

A less-known alternative approach used in ABL research is the stochastic model in which stochastic subgrid stress variations are added to a base SGS model. In Mason and Thomson (1992), these variations were added to the Smagorinsky–Lilly model. Results indicated an energy backscatter rate slightly larger than the dissipation rate, which would otherwise be disallowed in the Smagorinsky–Lilly model. Accordingly, there was a substantial improvement in the near-wall region of the flow, with a logarithmic profile.

2.3 Dynamic Models

All of the presented models to this point include at least one model coefficient that must be prescribed based on theoretical considerations (e.g., isotropy), empirical data, or chosen ad hoc to recover the "correct" a posteriori results from simulations. Germano et al. (1991) pioneered a procedure to dynamically calculate these unknown model coefficients, leading to the so-called dynamic model. An analogous procedure was first applied to scalars and compressible flows by Moin et al. (1991). In the dynamic procedure, a second filter (the test filter; denoted by $\overline{\cdots}$) is applied to Eq. 2 at a larger scale (e.g., 2Δ), which results in the Germano identity

$$L_{ij} = T_{ij} - \overline{\tau_{ij}} = \overline{\widetilde{u}_i \widetilde{u}_j} - \overline{\widetilde{u}_i}\,\overline{\widetilde{u}_j}, \tag{8}$$

where T_{ij} is the SFS stress at the 2Δ level. If it is assumed the same SFS model can be applied for the stress at Δ and $\alpha\Delta$ (e.g., 2Δ) it can be exploited to derive model coefficients for any base model. Lilly (1992) applied the dynamic procedure to the Smagorinsky–Lilly model. By minimizing the associated square error of this combination, Lilly arrived at the following expression for the model coefficient

$$C_S^2 = \frac{L_{ij} M_{ij}}{M_{ij} M_{ij}},$$

where

$$M_{ij} = 2\Delta^2 \left[\overline{|\widetilde{S}|\,\widetilde{S}_{ij}} - \alpha^2 \left|\overline{\widetilde{S}}\right| \overline{\widetilde{S}}_{ij} \right].$$

This procedure is not limited to the Lilly–Smagorinsky model and can be applied to other base SFS models with one (e.g., Wong and Lilly 1994) or more model coefficients (e.g., Anderson and Meneveau 1999). The above expression allows for a dynamically computed value of the Smagorinsky coefficient that is consistent with local-flow properties. This local form of the dynamic Smagorinsky coefficient is numerically unstable ($\pm C_S^2$) due to high time correlations of C_S^2 coupled with the fact that the instantaneous energy cascade can be forward or backward (Germano et al. 1991). Another reason for the numerical instability is related to the assumption that C_S^2 is constant over the filter width $\alpha\Delta$. In the absence of this assumption, the model error becomes a set of integral equations. Ghosal et al. (1995) overcame this by minimizing the integral version of the error to find C_S^2 everywhere using a variational method, which was both computationally expensive and complex. The more common approach is to enforce the Germano identity in an average sense. Typically, this average is enforced over some region of spatial homogeneity (e.g., over horizontal planes in a homogeneous boundary layer) which removes the C_S^2 oscillations and aids numerical stability. This spatial averaging presents an issue in heterogeneous flows since the assumptions underlying the averaging procedure are violated. One approach to deal with this issue is the Lagrangian dynamic

model (Meneveau et al. 1996), whose underlying idea is that the Germano identity should be enforced along fluid particle trajectories. A Lagrangian time scale controls how far back in time to average using first-order time and space estimates.

A second problematic assumption is that C_S^2 is scale invariant (i.e., the same model and model coefficients can be used for τ_{ij} and T_{ij}). While this assumption is generally reasonable provided that both filter scales Δ and $\alpha\Delta$ are within the inertial subrange of turbulence, it will likely be violated in some region of the flow for cases with at least one direction of flow anisotropy (e.g., the ABL). Porté-Agel et al. (2000) addressed this by developing a generalized dynamic model where C_S^2 is a function of scale and made the weaker assumption that C_S^2 follows a power-law distribution at the smallest resolved scales, e.g., $C_S^2(\alpha\Delta)/C_S^2(\Delta) = C_S^2(\alpha^2\Delta)/C_S^2(\alpha\Delta)$. Porté-Agel (2004) extended this procedure to introduce the first scalar scale-dependent model, and Bou-Zeid et al. (2005) combined Meneveau et al. (1996) and Porté-Agel et al. (2000) to develop a scale-dependent Lagrangian dynamic model for momentum transport. Results showed that near the lower boundary the dynamic coefficient is very sensitive to the local surface roughness and that this new model is better matched with experimental data than is the planar-averaged formulation. Stoll and Porté-Agel (2006b) applied scale-dependent Lagrangian dynamic SGS models for both momentum and scalars to neutrally stratified boundary layers over heterogeneous terrain. These models were able to accurately reproduce flow statistics and the spatial distributions of the Smagorinsky coefficients and the SGS Schmidt number in a self-consistent manner. In both studies and later in a detailed wind-tunnel study (Carper and Porté-Agel 2008), the need to locally determine coefficients in simulations of realistic ABLs was elucidated.

2.4 Land-Surface Flux Models

Given the inertial conditions typical of the atmospheric surface layer (ASL), applications of LES are overwhelmingly based upon wall-modelled closures predicated upon a TKE equilibrium condition (Pope 2000; Piomelli and Balaras 2002). The Monin–Obukhov similarity theory (Monin and Obukhov 1954, MOST) has figured prominently in the proliferation of LES for atmospheric turbulence modelling, owing to its practical convenience and reliability (Stoll and Porté-Agel 2006a). Within this framework, surface fluxes of momentum and heat are defined, respectively, via

$$\frac{\tau_{iz}^w(x,y,t)}{\rho} = u_*^2 = \left[\frac{\kappa U(\vec{x})}{\psi_m(\zeta)}\right]^2 \frac{\tilde{u}_i(\vec{x},t)}{U(\vec{x})}, \tag{9}$$

and

$$\frac{Q_0}{\rho C_p} = u_*\theta_* = \left[\frac{\kappa\delta\theta(\vec{x})}{\psi_h(\zeta)}\right] u_*, \tag{10}$$

where u_* is the friction velocity, κ is the von Kármán constant, $U(\vec{x}) = \left(\langle\tilde{u}(\vec{x},t)\rangle^2 + \langle\tilde{v}(\vec{x},t)\rangle^2\right)^{1/2}$ is the resolved velocity magnitude at the lowest computational level determined over horizontal planes, locally at each grid point, or as the local filtered value (Bou-Zeid et al. 2005; Stoll and Porté-Agel 2006a), $\psi_m(\zeta)$ and $\psi_h(\zeta)$ are the stability corrections, derived from vertical integration of the modelled non-dimensional gradients (Brutsaert 1982), where $\zeta = zL^{-1}$ is the stability parameter and $L = u_*^2\theta_0(\kappa g\theta_*)^{-1}$ is the Obukhov length determined in the same manner as $U(\vec{x})$, C_p is specific heat, θ_* is the so-called friction temperature, and $\delta\theta(\vec{x})$ is the local vertical thermal gradient responsible for convective heat fluxes. In this form, within the stability corrections, $\psi_m(\zeta)$ and $\psi_h(\zeta)$, enter pre-defined roughness

lengths, $z_{0,m}$ and $z_{0,h}$, and which represent the elevation at which ensemble-mean dependent quantities attain their surface values (Garratt 1992). For further discussion, interested readers may consult the recent reference text, Wyngaard (2010).

The wall-modelled LES paradigm offers the redeeming attribute that dependent flow quantities enter as input argument during integration of the transport equations, yielding corresponding surface fluxes (i.e., Eqs. 9 and 10). Equilibrium-contingent models have well-known limitations, foremost among them being application in a space–time local sense and limitations related to the application of MOST for values of $zz_{0,m}^{-1} < \mathcal{O}(10)$ in high-resolution simulations (Basu and Lacser 2017). Equations 9 and 10 have utility in modelling flow over landscapes that are horizontally homogeneous, e.g., types of agricultural fields, gently undulating topography, ice sheets, sand flats, etc. But their prognostic abilities break down with the introduction of relative larger-scale obstacles, for example, buildings, topographic undulations, sand dunes, vegetative canopies, etc. Such conditions necessitate generalized boundary conditions.

For flow over vegetative canopies, models based upon an a priori defined leaf-area index (LAI) can be added to Eq. 2 (e.g., for F_i) as a body force,

$$F_i = c_{\mathrm{D}} a(\vec{x}) \tilde{u}_i U(\vec{x}), \tag{11}$$

where

$$LAI = \int_{\mathrm{d}^2\vec{x}} a(\vec{x}) \mathrm{d}^2\vec{x}, c_{\mathrm{D}} \sim \mathcal{O}(10^0) \tag{12}$$

is a drag coefficient, and $a(\vec{x})$ is leaf-area density, which relates to LAI via the right-hand side integral in Eq. 12 (Shaw and Schumann 1992). Flows over non-porous obstacles, such as buildings or sharply varying terrain, are commonly based on an immersed-boundary method (IBM) (Peskin 1972; Mittal and Iaccarino 2005) – typically categorized as either a direct or indirect method. In applications to ABL turbulence, IBM schemes typically utilize a surface closure based on surface stress (Chester et al. 2007), or some other spatial attribute of the obstacle (Anderson and Meneveau 2010; Anderson 2012).

In other cases, the spatial variability of an underlying landscape is too steep to be captured within an equilibrium-like model (i.e., Eq. 9), solid, but not sufficiently steep to require an IBM closure. In such scenarios, the Cartesian computational domain can be mapped to a curvilinear domain—typically from z to η, via linear transformation. This mapping introduces new terms within the momentum transport equation solver, but precludes the need for additional body forces since topographic undulations vanish following the mapping procedure (Gal-Chen and Sommerville 1975; Clark 1977; Bao et al. 2018). It is noted, too, that solution of the mapped equations poses additional challenges for maintaining divergence-free velocity; in the Cartesian grid, divergence-free conditions are preserved via dynamic computation of a pressure correction, which is itself derived from solution of a Poisson equation. Though beyond the scope of this article, it is emphasized that solution of the mapped pressure Poisson equations requires careful treatment (Yang and Shen 2010). The aforementioned discussion addresses boundary-flux modelling for momentum, but LES modelling of non-neutral turbulence also requires special treatment of the corresponding heat and moisture boundary fluxes. We note, for example, early work on CBL flow over undulating terrain (Walko et al. 1992; Dörnbrack and Schumann 1993) and efforts to use land-surface models to represent the impact of the surface energy and mass budgets (Patton et al. 2005; Huang and Margulis 2010; Shao et al. 2013).

3 Applications in Boundary-Layer Research

3.1 The Convective Boundary-Layer

3.1.1 CBL Structure and Dynamics

Some of the earliest LES studies of the ABL focused on the daytime CBL (Deardorff 1970b, 1972a, 1974a, b). In a seminal paper, Deardorff (1972a) simulated neutral and convective ABLs, considering values of the global stability parameter $-z_i L^{-1} = 0, 1.5, 4.5, 45$, where z_i is the potential temperature inversion height. Deardorff demonstrated the validity of mixed-layer scaling, where the CBL depth is characterized by z_i (rather than the Ekman layer depth $u_* f^{-1}$), the stability parameter for the mixed layer is $-z_i L^{-1}$ (rather than $u_*(fL)^{-1}$), and the appropriate scales for normalizing statistics throughout the convective mixed layer are the convective velocity scale $w_* = (g z_i Q_0/\theta_0)^{1/3}$ and the convective temperature scale $T_* = Q_0 w_*^{-1}$. He also demonstrated that for weakly convective conditions (e.g. $-z_i L^{-1} = 4.5$), the velocity and temperature fields are organized in coherent streaks near the ground closely aligned to the mean wind direction; however, updrafts were found to be organized into open cells for more convective ($-z_i L^{-1} = 45$) conditions. Deardorff also presented preliminary results of dispersion in the CBL, demonstrating that vertical dispersion of neutrally buoyant particles increases with increasing $-z_i L^{-1}$.

Mason (1989) performed a suite of LES of free convection, investigating the extent to which grid resolution and details of the SGS model impact the fidelity of simulations. He found that the domain size and grid resolution had a significant impact, and proposed a modified eddy viscosity where the subgrid length scale was a function of the SGS Richardson number; this led to improved results in his simulations. Free convection was investigated further by Schmidt and Schumann (1989), with a focus on convective organization. In addition to considering vertical profiles of second- and third-order moments and velocity and temperature spectra and cospectra, they performed a detailed analysis of the coherent organization of the velocity and temperature fields and found that the vertical velocity and temperature fields organize into open cellular patterns (where several updrafts meet at a "hub"), with a horizontal length scale of $\sim 2z_i$, and with updrafts and downdrafts extending throughout the depth of the CBL.

Free convection also served as the basis for one of the first ABL LES intercomparison studies. Nieuwstadt et al. (1993) compared four different numerical simulation codes with different discretization schemes and SFS models. They found that even at the low resolution used ($\sim 6.4 \times 10^4$ grid points), profiles of boundary-layer statistics were consistent across the participating models demonstrating that LES could be reliably used to study ABL dynamics. The good agreement was attributed to the dominance of large-scale thermals that are easily resolved by LES. In a follow-up study using the same four numerical codes, Andren et al. (1994) examined the impact of shear using the case of a neutrally stratified Ekman layer. They found that with the absence of large-scale thermals the numerical codes showed significant deviations from each other and, based on sensitivity tests, that the differences where largely attributed to differences in SFS model formulation. Fedorovich et al. (2004) performed an intercomparison using forcing conditions that combined shear and convection in an attempt to understand some of the contradictory conclusions of previous work on CBL entrainment. They found relative consistency in ABL statistical profiles for first-order statistics with increasing scatter between numerical codes with increasing statistical order. The relatively good agreement among models compared to earlier intercomparisons could

have been a result of the significant increase in resolution afforded by a decade of time ($\sim 6.5 \times 10^6$ grid points) or because the inclusion of any convection with or without shear results in significant energy at resolved length scales.

Prior to Fedorovich et al. (2004), Moeng and Sullivan (1994) investigated the question of how buoyancy and shear together influence CBL structure and dynamics by running a suite of LES for $-z_i L^{-1} = 0, 1.4, 1.6,$ and 18 by independently varying the geostrophic wind speed U_g and the surface heat flux. They considered the instantaneous organization of the velocity field—finding similar results to Deardorff (1972a)—and additionally considered vertical profiles of second- and third-order moments, and the TKE budget. They proposed that the appropriate velocity scale for the moderately convective CBL could be formed from the convective velocity scale w_* and the friction velocity, i.e. $w_m^3 = w_*^3 + 5u_*^3$. The question of how the interplay of shear and buoyancy together impact the large-scale organization of the CBL was considered further by Khanna and Brasseur (1998), who simulated CBLs with stabilities ranging from $-z_i L^{-1} = 0.44$ to 730. Based on their analysis of LES results, they proposed a mechanism whereby the organization of warm fluid ($\theta' > 0$) in low-momentum streaks ($u' < 0$) under weakly convective (small $-z_i L^{-1}$) conditions leads to the development of horizontal convective rolls aligned 10°–20° to the left of the mean wind direction.

Large-eddy simulation also has been used to investigate the structure of the entrainment zone in the CBL (Sullivan et al. 1998; Conzemius and Fedorovich 2006; Kim et al. 2003), which is challenging to observe. Sullivan et al. (1998) performed LES of the shear-free CBL with grid nesting near the inversion layer, in order to investigate entrainment dynamics, and found that convective plumes play a key role in the entrainment process. For weakly stratified inversion zones (low *Ri*), rotational motions due to penetrating convective plumes led to folding of the inversion interface; however, stronger stratification (larger *Ri*) prevented this folding, and smaller-scale turbulent mixing led to the entrainment of warm air. Conzemius and Fedorovich (2006) conducted a suite of LES experiments to study how the dynamics of the entrainment layer and associated CBL development were affected by the presence of shear. They found that entrainment zone shear played a larger role in enhancing CBL entrainment than did surface shear. The authors in op. cit. also showed that the sheared entrainment zone exhibited a layer where shear and buoyancy effects were balanced, which regulated the CBL entrainment. Kim et al. (2003) focused on entrainment in the sheared CBL (the entrainment heat flux is known to be larger under sheared convective), and found strong linear vortices occur in the entrainment layer for sheared convection, with locations coinciding with those of horizontal convective rolls. Furthermore, Kelvin–Helmholtz (K–H) wave-like billows were found in the entrainment layer, over strong updraft regions; the K–H billows were found to lead to the enhanced entrainment heat flux in sheared convection.

Other LES studies of the CBL have considered diverse topics, such as the extent to which baroclinicity affects mean vertical profiles and turbulence (Sorbjan 2004) and the validity of (and deviations from) MOST under convective conditions (e.g., Khanna and Brasseur 1997; Li et al. 2018). These studies have indicated the potential influence of an additional dimensionless parameter related to the outer length scale (i.e. zz_i^{-1}) and suggested that coherent updrafts and downdrafts may be responsible for deviations from MOST. Large-eddy simulation was used by Kanda et al. (2004a) to investigate surface energy balance closure in the CBL; they found that the temporally averaged sensible heat flux ($\langle w'\theta' \rangle$) systematically underestimated the horizontally spatially averaged heat flux, which led to a systematic bias in the surface energy budget. Other studies have used LES to investigate and characterize the statistics associated with CBL turbulence (e.g., Gibbs and Fedorovich 2014a, b).

Sullivan and Patton (2011) revisited the question of the extent to which grid resolution affects CBL statistics in LES, performing simulations of the shear-free CBL at resolutions

ranging from 32^3 to 1024^3. They found that filter widths $\Delta < z_i/60$ (corresponding to their 256^3 simulations) were necessary to obtain statistical convergence for first- and second-order moments in the interior ($0.1 \leq z z_i^{-1} \leq 0.9$) of the domain. Furthermore, they found estimation of vertical velocity skewness required filter widths of $\Delta < z_i/113$. While Sullivan and Patton (2011) employed a subgrid model based on solution to the SGS TKE equation, grid convergence tests using other SGS models (e.g. Salesky et al. 2017) indicate that grid resolution requirements for accurate LES of the CBL are sensitive to the choice of SGS model.

Recently Salesky et al. (2017) used LES to investigate the transition from horizontal convective rolls to open cells in the CBL (and the associated implications for momentum and heat transport). Large-eddy simulation has also been used to examine the extent to which the topology of large- and very-large-scale motions (which are well-characterized in neutrally stratified engineering flows, Hutchins and Marusic 2007) is modified by buoyancy, and how these structures modulate the amplitude of small-scale turbulent fluctuations in the CBL with increasing unstable stratification (Salesky and Anderson 2018), corroborating studies based on aircraft observations (Lemone 1976).

3.1.2 CBL Modelling and Parametrization

In addition to being used to advance the community's understanding of the CBL, LES has also been used extensively to develop, validate, and improve parametrizations of the CBL for numerical weather prediction models. Vertical transport in the CBL is asymmetric, due to the positive skewness of vertical velocity ($\mathrm{Sk}(w) = \langle w'^3 \rangle \langle w'^2 \rangle^{-3/2} > 0$) which arises because the flow field is comprised of intense updrafts that take up a small volume fraction of the flow, and larger regions of less intense downdrafts. Notably, heat and scalar fluxes (e.g. $\langle w'\theta' \rangle$) in the convective mixed layer occur in spite of negligible mean temperature or scalar gradients (e.g. $\partial \langle \theta \rangle / \partial z$), meaning that the typical approach of modelling the flux through an eddy diffusivity, i.e.

$$\langle w'\theta' \rangle = -K_\theta \frac{\partial \langle \Theta \rangle}{\partial z} \tag{13}$$

fails in the mixed layer, since the eddy diffusivity K_θ becomes ill-defined as $\partial \langle \theta \rangle / \partial z \to 0$. In order to ameliorate this issue, a number of investigators have used LES to explore alternatives or extensions to K-theory in the CBL.

Work by several authors (Wyngaard and Brost 1984; Moeng and Wyngaard 1989; Wyngaard and Weil 1991) investigated conserved passive scalars in the CBL. Notably, Moeng and Wyngaard (1989) was the first study to compare results from second-order CBL parametrizations schemes with LES data. The authors found, among other things, that downgradient diffusion closures for turbulent transport were inadequate due to the influence of buoyancy in the CBL. In total, these studies demonstrated that conserved passive scalar statistics can be represented as a superposition of "bottom-up" processes (due to upward transport and mixing) and "top-down" processes, related to entrainment. A key finding was that the top-down scalar flux ($\langle w'\theta' \rangle_t$) has a well-behaved turbulent diffusivity, but the turbulence diffusivity of the bottom-up scalar flux ($\langle w'\theta' \rangle_b$) has a singularity in the mixed layer. Wyngaard and Weil (1991) proposed that nonlocal bottom-up scalar transport (i.e. due to updrafts) could be modelled in terms of the vertical velocity skewness $\mathrm{Sk}(w)$ and the vertical gradient of the scalar flux, $\partial \langle w'\theta' \rangle / \partial z$.

Ebert et al. (1989) proposed to represent nonlocal transport in the CBL in terms of what they referred to as transilince theory, where nonlocal mixing can be represented by a matrix of

mixing (or transilience) coefficients $\left[c_{ij}(t, \Delta t)\right]$ that represent the fraction of air that travels from source level i to destination level j over some time period Δt; LES was used to evaluate these mixing coefficients. They found significant asymmetry in vertical mixing; over several large-eddy turnover times, the mixing coefficients indicated removal of nearly all surface air, with a large amount of slow downward transport. As indicated by other studies, Ebert et al. (1989) found that K-theory breaks down for vertical transport in the CBL.

Building upon ideas presented in Deardorff (1972b), Holtslag and Moeng (1991) proposed including a counter-gradient term in the bottom-up eddy diffusivity for heat,

$$\langle w'\theta' \rangle = -K_\theta \left(\frac{\partial \langle \theta \rangle}{\partial z} - \gamma_\theta \right) \tag{14}$$

where the counter-gradient term $\gamma_\theta = C\langle w'\theta' \rangle_0 / w_* h$ can be related to the surface flux $\langle w'\theta' \rangle_0$. Using LES, they demonstrated that the bottom-up scalar diffusivity is well-behaved when the counter-gradient term is included, meaning that an equation of the form of Eq. 14 could be implemented in weather forecasting models.

Other studies have used LES to develop CBL parametrizations based on a mass-flux type approach (e.g. Randall et al. 1992; Siebesma et al. 2007), which considers the vertical transport (of heat or scalar) due to updrafts or downdrafts. This is typically accomplished by including an additional term in the eddy diffusivity formulation (Siebesma et al. 2007), i.e.

$$\langle w'\theta' \rangle = -K_\theta \frac{\partial \langle \theta \rangle}{\partial z} + M(\theta_u - \langle \theta \rangle) \tag{15}$$

where M is the mass flux and θ_u is the potential temperature in updraft regions. The mass flux and updraft fraction in Eq. 15 can be evaluated directly from LES output to inform the development of weather and climate model parametrizations.

Ayotte et al. (1996) also used LES to evaluate the fidelity of CBL closure models for use in weather and climate forecasting. They ran a suite of 10 simulations of the CBL encompassing free convection, sheared convection, the baroclinic CBL, and an Ekman layer simulation. Several classes of CBL closure models were evaluated, including those where the eddy viscosity was specified as a function of stability (i.e. $K(Ri)$), K-profile models, mixed-layer models, Mellor–Yamada 2.0- and 2.5- order closure models, and a transilience model. The authors noted that the closure models had significantly different treatment of the entrainment zone, leading to widely varying prediction of quantities in the mixed layer. Thus, LES of the CBL has become instrumental as a tool for developing new parametrizations.

3.2 The Stable Boundary-Layer

The study of the stratified ABL has been an area of continuous interest since the emergence (around 1990) of LES as a prominent technique for investigating ABL turbulence. A common thread has been a focus on the capability of LES to faithfully represent the physics of turbulent transport in the presence of stratification. The challenge lies in the representation of the SFS stress and flux under weak turbulence conditions when typical SFS model assumptions including isotropic behavior at the filter scale are not valid.

The first LES of the SBL was performed by Mason and Derbyshire (1990). A basic domain and simulation forcing was used that effectively consisted of a pressure driven channel-flow simulation with a negative sensible heat flux prescribed at the surface. The adopted modelling strategy was very similar to previous simulations of neutral (Mason and Callen 1986) and convective (Mason 1989) boundary-layers and used the Smagorinsky–Lilly closure (Eq. 6).

The primary modification to the SGS model for SBL simulations was the inclusion of a *Ri*-based stability correction. This idea had been introduced previously (e.g., Deardorff 1980) but this is one of the earliest instances specifically for the purpose of simulating stratified turbulence. Although some aspects of the simulation set-up were later shown to be undesirable (e.g., constant flux surface boundary conditions discussed in Basu et al. 2008a; Gibbs et al. 2015), basic agreement between theory (i.e., Nieuwstadt 1984) and the simulation results established that LES of the SBL was possible.

Since these first SBL simulations, considerable effort has focused on the development and validation of SGS models. Brown et al. (1994) tested the stochastic backscatter model of Mason and Thomson (1992) in SBL LES and concluded that the inclusion of backscatter in the SGS model improved the agreement with the local-scaling hypothesis (Nieuwstadt 1984) by preventing the local collapse of turbulence that can occur in poorly resolved regions of a SBL with standard versions of the Smagorinsky–Lilly closure. Andren (1995) and Galmarini et al. (1998) examined the fidelity of higher-order closure models that were effectively LES versions of the Mellor and Yamada (1974) 1.0 closure. These models closely resembled the model introduced by Sullivan et al. (1994) with SBL specific SGS flux corrections. Both found that the inclusion of prognostic equations for the SGS fluxes improved agreement with local scaling and alleviated the need for a stochastic component. Saiki et al. (2000) directly implemented the model of Sullivan et al. (1994) with the SGS length scale modified following Deardorff (1980). Although a significant number of early LES of the SBL used a length scale of the form $\ell = \min\left(\Delta, 1/2\sqrt{E}N^{-1}\right)$, recent work has indicated that this is likely incorrect for anything but very coarse resolution LES (Gibbs and Fedorovich 2016). Saiki et al. (2000) used a similar simulation set-up to past work but with a significantly larger geostrophic wind speed and a larger domain. Besides reporting that modifications to the original scheme improved agreement with theory, Saiki et al. (2000) reported on wave interactions at the boundary-layer top and the impact of these interactions on the structure of flow in the boundary-layer. This was not the first reporting of wave–turbulence interactions (e.g., Andren 1995) but it was an early example of a transition from the majority of work in the 1990s focusing on the ability of LES to represent the SBL to an examination of SBL physics.

The transition to using LES as a research tool to examine SBL physics coincided with a move towards the simulation of quasi-steady SBLs with conditions inspired by ABL observations. Pioneering in these efforts was Kosović and Curry (2000) who used data from the Beaufort Sea Arctic Stratus Experiment to motivate an ensemble of LESs with a short enough inertial oscillation period to reach equilibrium fast enough with the computational power available at the time. These simulations can be viewed as delineating a break between ABL LES of stratified turbulence and the channel flow simulations favored in the engineering literature at the time (e.g., Armenio and Sarkar 2002).

The most important lasting contribution of Kosović and Curry (2000) is that their simulation set-up became the basis for the first intercomparison of LES models for the SBL as part of the Global Energy and Water Exchanges (GEWEX) ABL study (GABLS1, Beare et al. 2006). The intercomparison examined the performance of 11 different LES models with various numerics and SGS modelling schemes. The simulations were run for a range of resolutions (depending on participants) and compared to theory, field data, and a high resolution "benchmark" case. The study found that for moderate stratification ($L\delta^{-1} \approx 1.5$, where δ is the boundary-layer height), LES can successfully represent the quasi-steady SBL. This conclusion was based on the relative convergence of results from the various LES models at a sufficient resolution and the agreement of the ensemble of simulations with data and theory.

The GABLS1 intercomparison established a strong basis for the use of LES to examine weak to moderately stable ABLs and became a benchmark for the evaluation of single column models (Cuxart et al. 2006; Svensson and Holtslag 2009), the development of LES SGS models (e.g., Stoll and Porté-Agel 2008; Matheou and Chung 2014), and for the examination of turbulent fluxes (e.g., Basu et al. 2006; Steeneveld et al. 2007; Huang and Bou-Zeid 2013; Sullivan et al. 2016). While SGS model development continued, this also marked a transition to using LES to examine the physics of turbulence and towards increasingly complex simulation scenarios. For example, Basu et al. (2006) combined results from the GABLS1 study with field data to examine the applicability of MOST and Steeneveld et al. (2007) used the GABLS1 results with experimental data to evaluate diagnostic models for boundary-layer height. Huang and Bou-Zeid (2013) used the GABLS1 case as a basis for an expanded study of the impact of stratification on the structure of the ABL. Besides general observations of the impact of increasing stratification on boundary-layer depth and transport characteristics, they also examined the local-scaling hypothesis and found that the concept of z-less scaling (Mahrt 1999) applied at a lower level than typically assumed. Sullivan et al. (2016) used very high resolution simulations of the GALBS1 case for a detailed examination of the structure of turbulence in the SBL. They identified three-dimensional inclined vortical structures similar to those identified in the neutral ABL (e.g., Carper and Porté-Agel 2004) and linked these to temperature ramps observed in the simulations and in field studies.

Researchers also began to add a wider range of atmospheric forcing conditions to their simulations to explore the implications on boundary-layer dynamics and modelling. Mirocha and Kosović (2010) used LES to analyze the impact of subsidence on mixing in the SBL. The simulations were motivated by field observations and demonstrated that even very weak subsidence can have a strong impact by limiting the growth of the boundary-layer and significantly reducing mixing and cooling in the boundary-layer. Additionally, they found that the inclusion of subsidence improved the agreement between simulations and observations. Richardson et al. (2013) created a SBL LES database that included a wide range of atmospheric forcing conditions to examine boundary-layer-height formulations. Most recently, LES SBL work has transitioned towards the very stable ABL with simulation of long-lived boundary layers in Antarctica at Dome C Station (van der Linden et al. 2019). These simulations demonstrated that LES can move into the space of very stable boundary layers but only at the expense of very high resolution.

3.3 Transitional ABL

In addition to studies of the structure and dynamics of the CBL and SBL under quasi-steady forcing, LES has also been used to understand the details of the morning transition, evening transition, and full diurnal cycle of the ABL.

Sorbjan (2007) considered growth of the CBL through the morning transition, by simulating an initially shallow CBL and forcing simulations with an increasing surface heat flux. He demonstrated that the mean wind shear and temperature gradients remained constant throughout the lower half of the mixed layer, but evolved in time in the upper half of the mixed layer and interfacial layer due to entrainment. Beare (2008) investigated the full morning transition from a SBL to a CBL by spinning up SBL simulations on a smaller domain, then using this as the initial condition for the morning transition. The morning transition was found to be highly sensitive to shear in its early stages, and a so-called "mixed CBL–SBL" was observed, where a shallow CBL was capped by a shear-driven SBL. Beare found that

the depth of the overlying SBL increased with increasing geostrophic wind speed, indicating that the SBL cannot be neglected in understanding or modelling the morning transition.

Nieuwstadt and Brost (1986) considered the decay of turbulence in the CBL by running LES to reach steady state, then abruptly setting the surface heat flux to zero. They found that the temperature variance $\langle \theta'^2 \rangle$ decayed first (from the bottom up), followed by the vertical heat flux $\langle w'\theta' \rangle$ (also from the bottom up), the vertical velocity variance $\langle w'^2 \rangle$, and finally the horizontal velocity variances $\langle u'^2 \rangle$ and $\langle v'^2 \rangle$. The ratio of time to the large-eddy turnover time $t/T_L = t w_*/z_i$ was found to be the appropriate time scale to characterize the decay process. Sorbjan (1997) considered the more realistic case of a gradually decreasing surface heat flux, demonstrating that the decay rate of TKE depended on the both the rate of decrease of the surface heat flux and the large-eddy turnover time scale w_*/z_i. Pino et al. (2006) also considered the evening transition (focusing on the sheared CBL), finding that wind shear increased entrainment during the transition, and that the horizontal velocity variances decay much more slowly than the vertical velocity variance, leading to an increase of anisotropy during the transition.

The first LES of the full diurnal cycle was performed by Kumar et al. (2006), using idealized time series of surface heat flux $\overline{w'\theta'}_0$ and geostrophic wind speed U_g derived from surface observations as forcings. They found that simulation results produced good agreement with expected behaviour of entrainment, CBL growth, and development of a nocturnal jet. They also found that velocity variances, TKE, and the dynamically calculated Smagorinsky coefficient C_S exhibited hysteresis-like behaviour when normalized by ΔL^{-1}; however, this hysteresis was negligible when statistics were normalized by $\Delta \Lambda^{-1}$, where Λ is the local Obukhov length (Nieuwstadt 1984), strongly supporting Nieuwstadt's local scaling hypothesis. Basu et al. (2008b) used a locally averaged version of the dynamic model for both momentum and heat SGS fluxes (Kumar et al. 2006, only used the model for momentum) and found that it was able to accurately capture behaviour of the diurnal transition of the ABL. Later, Kumar et al. (2010) investigated the impact of surface boundary conditions and geostrophic forcing on the simulated diurnal evolution of the ABL, finding that some combinations of forcings are superior for recovering CBL statistics, and others for capturing the nocturnal SBL. They found that imposing a surface temperature (rather than a surface heat flux) better captured the fluxes and night-time profiles (in agreement with Basu et al. 2008a), but concluded that coupling with a surface energy balance model would be necessary to generally improve agreement between simulations and observations.

3.4 Plant Canopy Flows

Not long after LES became a widespread technique for the study of the ABL, researchers started to simulate the dynamics of plant canopy flows (Shaw and Schumann 1992). Although these first simulations used a relatively small domain, combined with simulations of Kanda and Hino (1994) and Su et al. (1998), this early work on LES of canopy flows established the ability of LES to reproduce some of the most salient features of canopy-induced turbulence and the basic models and simulation forcing parameters required.

The basic methodology used to represent the canopy has remained largely consistent with Eq. 11 but researchers have proposed different ways to represent both canopy drag and the impact of unresolved interactions of the flow with the plant canopy. Those using a form of Eq. 7 (e.g., Shaw and Schumann 1992; Kanda and Hino 1994; Dwyer et al. 1997) introduced an energy sink term into the equation to represent the impact of energy dissipation due to unresolved plant matter. The addition of the term is consistent with the general idea of a

spectral "short circuit" of energy (Finnigan 2000; Shaw and Patton 2003) from large to small scales with the form of the term closely following higher-order RANS closures for plant canopies (Wilson 1988). Shaw and Patton (2003) found that the form of this term is not critical within a plant canopy as a result of SFS wake energy's small value compared to resolved TKE and SFS kinetic energy. Other researchers have also developed methods to include unresolved or poorly resolved impacts of individual canopy components. Yue et al. (2007) developed a drag model that included a classical cylinder drag component to account for subgrid (but still significant) drag from the trunk of a plant and Shaw and Patton (2003) included the effect of viscous (boundary-layer) drag on leaf surfaces. Shaw and Patton (2003) found the viscous drag component to be unimportant compared to form drag and the model of Yue et al. (2007) never found favour with modellers. A more sophisticated approach was developed for fractal trees by Chester et al. (2007) using an IBM to represent the resolved portion of a tree and then assuming the tree is fractal, the SGS drag was estimated. This method has the novel feature that it includes the impact of sheltering at unresolved scales but it has not caught on outside the research group it was developed in likely because drag from real trees is mostly considered to be a result of the leaf-area density and in general, the distribution of leaf sizes is not fractal. An IBM approach was also employed by Yan et al. (2017) and compared to wind-tunnel data from a model deciduous canopy. They found that a combination of an IBM model for the trunk and a porous canopy drag model (e.g., Eq. 11) provide the best representation. Besides capturing drag due to unresolved plant components, significant effort has examined the impact of plant motion on momentum transport (e.g., Dupont et al. 2010).

The development and maturation of plant canopy LES coincided with advancements in the experimental and theoretical understanding of canopy flows. Two topics stand out from the experimental and theoretical work, the origin and role of scalar microfronts over plant canopies and the "mixing-layer" analogy. Scalar microfronts are clearly identifiable ramp structures found most commonly in temperature time-series just above a plant canopy (e.g., Gao et al. 1989) and the "mixing-layer" analogy hypothesizes on the dominant transport mechanism between a plant canopy and the ASL by comparisons with classical mixing-layer theory (Raupach et al. 1996). LES has played a critical role in elucidating these two ideas and how they are linked through turbulent flow structures. This started with Kanda and Hino (1994) who examined the evolution of instantaneous canopy-top structures and their link to TKE and vertical momentum fluxes. They identified two primary canopy-top structures (spanwise vortical "rolls" and streamwise vortical "ribs") and associated vertical profiles of Reynolds stress and turbulence intensity with inclined structures above the canopy. Fitzmaurice et al. (2004) extended this by releasing a passive scalar and examining the correlation of scalar ramps with pressure perturbations. They found that scalar ramp structures coincided with positive peaks in the pressure and used conditional sampling to associate the ramp structures and pressure peaks with an upstream sweep zone and a downstream ejection zone. The association between pressure and scalar ramps is consistent with field data and using LES; Fitzmaurice et al. (2004) was able to add an understanding of the 3D velocity field associated with these ramps. Instead of conditionally sampling based on pressure, Watanabe (2004) used wavelet transforms to directly identify the scalar ramps. Watanabe (2004) confirmed prior results and also identified a link between canopy-top structures and streaks of low-speed momentum similar to those identified in boundary-layer flows (e.g., Hutchins and Marusic 2007). Future researchers would build on these ideas and continue to use LES to examine the link among scalar ramps, the mixing-layer analogy, and 3D coherent velocity structures. Finnigan et al. (2009) used the conditional averaging technique of Fitzmaurice et al. (2004) in a more extensive study of coherent structures and their evolution over a plant canopy.

They extended past work by analyzing λ_2', the second eigenvalue of the perturbation velocity gradient tensor (i.e., the velocity gradient tensor with the mean gradient removed), and the evolution of the conditionally sampled structures. They identified a highly 3D structure associated with head-up ejection generating and head-down sweep generating hairpin vorticies and surmised that these structures result from a helical pairing associated with the instability created by the canopy top velocity inflection and that this process is largely independent of the overlying turbulence in the ASL.

In a follow up, Bailey and Stoll (2016) used a similar simulation configuration to Finnigan et al. (2009) but with structure identification from the full velocity gradient tensor (e.g., λ_2 following Jeong and Hussain 1995). Based on conditional averages triggered on pressure perturbations, they developed an alternative theory on the evolution and form of canopy top coherent structures. They found a quasi 2D structure with 3D structures similar to Finnigan et al. (2009) superimposed on it. This was primarily a consequence of identifying structures based on λ_2 instead of λ_2' (see Bailey and Stoll 2016, appendix for a discussion of the difference in canopy structures identified with each). Additionally, they proposed a translative instability not helical pairing as the primary driver of canopy flow structures and that this instability aligns with hairpin "packets" (Adrian et al. 2000) and large-scale boundary-layer streaks (Hutchins and Marusic 2007) in the ASL above the canopy.

Similar to other application areas, once LES was established as a viable method to examine plant canopy flows researchers quickly moved on to more realistic forcing, domains, and canopy characteristics and interactions. Central to this was the inclusion of horizontal canopy heterogeneity. Although not technically a plant canopy, the work of Patton et al. (1998) on windbreak flows was one of the first to include horizontally heterogeneous porous elements modelled using Eq. 11. Researchers also focused on the impact of forest clearings and edges on canopy flow. For example, Cassiani et al. (2008) examined both clearing-to-forest and forest-to-clearing transitions with different LAI values and identified re-circulation zones at each transition. Dupont and Brunet (2008) validated their simulations of a clearing to forest transition and showed how increases in canopy density (LAI) shorten the adjustment zone over which turbulence develops compared to lower density cases.

After these somewhat idealized cases, researchers moved to more complex canopy architectures with ever increasing realism. Bohrer et al. (2009) was one of the first to look at a realistic horizontal distribution of leaf area density by combining coarse airborne lidar with a canopy reconstruction model. They found that heterogeneity had a strong impact in the vicinity of the canopy with a marked increase in flux spatial correlations. Although idealized, Bailey and Stoll (2013), and Bailey et al. (2014) simulated row-oriented crops (e.g., a grape vineyard) with resolved rows and examined the impact of this heterogeneity in the limit of a sparse canopy. Comparisons between row-resolved and the equivalent homogeneous canopy (i.e., equal LAI) found that horizontal heterogeneity has minimal impact on first-order statistics but a significant impact on higher-order statistics and canopy flow structures. In particular it increases second- and third-order statistical quantities, decreases the coherence of the flow, and both preferentially locates flow structures and for lower effective LAI, allows structures to penetrate deeper into the canopy. Boudreault et al. (2017) found similar impacts to Bailey and Stoll (2013) when using lidar data to examine forest-edge flow. The inclusion of realistic heterogeneity increased structure penetration at the edge and enhanced second- and third-order velocity statistics.

The inclusion of improved canopy architecture was also accompanied by efforts to improve and study the impact of more realistic forcing conditions and coupled canopy-atmosphere exchanges. General diurnal effects of plant canopies (Aumond et al. 2013) and detailed assessment of the impact of convection on turbulence statistics, coherent structures, and

canopy atmosphere interactions (Huang et al. 2009; Patton et al. 2016) where all studied. More recently, the impact of canopy heterogeneity and diurnal forcing conditions have been combined in simulations of a realistic semi-arid forest (Kröniger et al. 2018).

3.5 Dispersion and Urban Flows

Due to its importance for air quality and human health (Fenger 1999; Zhang et al. 2015), and its impact on both the ABL and large-scale weather systems (Hildebrand and Ackerman 1984; Shepherd 2005; Niyogi et al. 2011), urban meteorology has long been a topic of interest; LES investigations of the urban boundary layer (UBL) started in the early 2000s. Notably, LES was first applied to urban meteorology several decades later than canonical ABL flows, due to the additional complexity required to resolve the impacts of individual buildings on momentum and scalar transport. The earliest urban LES studies used finite volume or finite element methods with boundary-fitted grids (Hanna et al. 2002; Walton and Cheng 2002). IBMs have become popular recently (Tseng et al. 2006; Bou-Zeid et al. 2009; Giometto et al. 2017) due to their relatively low computational expense, and the fact that one can retain an underlying discretization on a Cartesian grid.

3.5.1 Urban Meteorology

In contrast to the ABL over flat, horizontally homogeneous terrain, the urban canopy layer (UCL) features additional complexities, including: (1) reduced mean wind speeds within the UCL due to drag forces on buildings, (2) a region of elevated shear at the top of the UCL, (3) production of small-scale turbulence in the wake of buildings, (4) significant spatial heterogeneity in the flow, which leads to additional terms (i.e. dispersive stresses and fluxes) in the governing equations, (5) a complex surface energy budget with heterogeneous heating and cooling of the ground and building walls, and (6) heterogeneous sources and sinks of scalars (water vapour, greenhouse gases, aerosols, etc.). These complexities make the collection and interpretation of field data extremely challenging (Pardyjak and Stoll 2017). In contrast, LES is free from many of the limitations of measurement systems and ideally suited for UBL studies.

The majority of urban LES studies have focused on urban street canyons (e.g. Walton and Cheng 2002; Cui et al. 2004) or arrays of cuboids (e.g. Kanda et al. 2004b; Kanda 2006; Philips et al. 2013) (typical of European and North American cities, respectively); a particular topic of interest in many urban LES studies is the extent to which geometric properties, such as the aspect ratio of street canyons or height distribution, alignment, and packing density of cuboids, influence the mean flow, turbulence, and scalar dispersion (e.g. Li et al. 2008; Cai et al. 2008; Hayati et al. 2019). Other studies have employed more realistic urban geometries (e.g. Tseng et al. 2006; Xie and Castro 2009; Bou-Zeid et al. 2009; Xie 2011; Kanda et al. 2013; Giometto et al. 2016) and recently, high-resolution LES with a significant degree of realism (Giometto et al. 2017) has become possible using techniques like airborne lidar that can measure urban geometry including tress and buildings at sub-meter resolution.

Early LES work on the UBL focused on characterizing the mean wind profile and turbulence statistics (velocity variances, turbulent kinetic energy, and momentum fluxes) in idealized urban geometries (e.g. Hanna et al. 2002; Kanda et al. 2004b). These simulations demonstrated that the mean velocity profile is greatly attenuated within the UCL, and the magnitude of the streamwise momentum flux $\langle u'w' \rangle$ peaks near the canopy top. Kanda et al. (2004b) demonstrated that the streamwise and vertical velocity variances (σ_u/u_* and σ_w/u_*,

respectively) change significantly with height inside the canopy; the maximum values of σ_u/u_* and σ_w/u_* within the canopy were found to increase with increasing plan area fraction $\lambda_p = A_p/A_T$ (where A_p is the planar area of buildings and A_T is the total area). Subsequent work used LES to characterize coherent structures in urban canopies (Cui et al. 2004; Kanda et al. 2004b; Kanda 2006). Kanda et al. (2004b) showed that the streamwise wavelength of coherent structures at the urban canopy top was $\lambda_x/H \approx 5$ for sparsely spaced cuboids (larger than what is found in vegetation canopies), and increases with increasing plan area fraction λ_p. These large streamwise wavelengths indicate that the mixing-layer analogy (Raupach et al. 1996) should not be expected to hold in urban canopies to the extent that it does in vegetation canopies. Using LES, Kanda (2006) demonstrated that the ratio of sweep ($u' > 0, w' < 0$) to ejection ($u' < 0, w' > 0$) events (i.e. S_2/S_4) in urban canopies was a factor of two larger than what has been measured in vegetation canopies.

In urban canopies and vegetation canopies, variables can be decomposed into a temporal mean and fluctuation, e.g. $u_i = \overline{u_i} + u_i'$ and a spatial mean and fluctuation, e.g. $u_i = \langle u_i \rangle + u_i''$ (Finnigan 2000), due to spatial heterogeneities in the flow. One can derive the mean momentum balance equation by double averaging (in time and space), yielding

$$\frac{\partial \langle \overline{u_i} \rangle}{\partial t} + \langle \overline{u_j} \rangle \frac{\partial \langle \overline{u_i} \rangle}{\partial x_j} = -\frac{1}{\rho}\frac{\partial \langle \overline{p} \rangle}{\partial x_i} - \frac{\partial \langle \overline{u_i' u_j'} \rangle}{\partial x_j} - \frac{\partial \langle \overline{u_i'' u_j''} \rangle}{\partial x_j} + f_{F_i} + f_{V_i} \tag{16}$$

where f_{F_i} and f_{V_i} correspond to form drag and viscous drag, respectively. Here terms emerge containing both the Reynolds stress, $\langle \overline{u_i' u_j'} \rangle$ (due to fluctuations from the temporal mean) and the so-called dispersive stress, $\langle \overline{u_i'' u_j''} \rangle$ (due to fluctuations from the spatial mean). Although the importance of dispersive stresses (and the corresponding scalar fluxes, e.g. $\langle \overline{u_i'' \theta''} \rangle$) has long been surmised in urban canopies, they can only be calculated from spatially resolved measurements. Large-eddy simulation studies (Kanda et al. 2004b; Xie and Castro 2006; Boppana et al. 2010) of flow and dispersion in urban geometry have demonstrated that the dispersive momentum ($\langle \overline{u'' w''} \rangle$) and scalar ($\langle \overline{\theta'' w''} \rangle$) fluxes can be significant within the UCL, accounting for 30% or more of the total flux within the canopy. In simulations of flow over Basel, Switzerland, Giometto et al. (2016) found that dispersive fluxes varied significantly in space; furthermore dispersive transport in the TKE budget was found to be non-negligible within the UCL.

Investigators have also found LES to be a valuable tool for developing urban parametrizations for large-scale weather and climate models. The mean velocity profile for a neutrally stratified ASL over a rough surface, above the roughness sublayer, is given as

$$\overline{U}(z) = \frac{u_*}{\kappa} \ln\left(\frac{z-d}{z_{0,m}}\right), \tag{17}$$

where d is the displacement height. An important question for urban parametrizations is how aerodynamic parameters ($z_{0,m}$ and d) are related to properties of the urban morphology (Grimmond and Oke 1999), such as the mean building height ($\langle h \rangle$), maximum building height (h_{max}), standard deviation and skewness of building height (σ_h and Sk_h), and the plan-area and frontal area fractions λ_p and $\lambda_f = A_f/A_T$ (where A_f is the frontal area of buildings projected in the mean wind direction). Kanda et al. (2013) ran an ensemble of over 100 simulations of real urban areas (focusing on subsets of Tokyo) to create a database of turbulence statistics and surface drag corresponding to various surface morphologies. Using the database, they proposed parametrizations for $z_{0,m}$ and d as a function of $\langle h \rangle$, h_{max}, σ_h, λ_p, and λ_f. Zhu et al. (2017) performed LES over synthetic urban geometry, demonstrating that $z_{0,m}$ also has a non-trivial dependence on Sk_h, the skewness of the building height

distribution. Other work (Sadique et al. 2017) has focused on how $z_{0,m}$ is related to building aspect ratio by including a model for sheltering, i.e. a reduction of momentum in the wakes of individual buildings, which affects the drag on surrounding buildings (Raupach 1992).

In vegetation or urban canopies, the mean velocity profile within the canopy is often assumed to follow an exponential profile (Macdonald 2000), i.e.,

$$U(z) = U_h \exp\left[a(z/h - 1)\right], \quad z \leq h, \tag{18}$$

where U_h is the wind speed at canopy top, h is the canopy height, and a is an extinction coefficient taken to be proportional to LAI (in vegetation canopies) or frontal area fraction λ_f in urban canopies. Large-eddy simulation has been used to investigate the extent to which Eq. 18 (and the underlying assumptions) hold in urban canopies (Castro 2017). To derive Eq. 18, one must assume a constant drag coefficient C_d with height within the canopy, that the Reynolds stress can be modelled with a mixing length model (i.e. $-\langle u'w' \rangle = l_m^2 (\partial U/\partial z)^2$) where the mixing length is constant with height, and that dispersive stresses can be neglected (Castro 2017). However, LES studies have demonstrated that both C_d and l_m have non-negligible variation with height within the urban canopy, meaning that Eq. 18 does not hold true in general in urban canopies.

Large-eddy simulation has also been used to investigate the extent to which buoyancy modifies flow and transport in urban canopies with simulations where the ground (Li et al. 2010; Boppana et al. 2014; Tomas et al. 2016) or walls (Cai 2012) are heated or cooled in order to assess the impacts of stratification on the mean velocity profile, turbulence statistics, residence time of pollutants released in street canyons, and strength and structures of mean vortex circulations in street canyons. Recently, LES has been coupled with energy balance models for urban areas in order to impose a realistic distribution of building surface temperatures and to investigate the diurnal evolution of flow within the urban canopy (Yaghoobian and Kleissl 2014; Nazarian et al. 2018).

An important question related to our ability to describe the geometry of urban areas is the sensitivity of simulated urban flows to the details of urban geometry. Bou-Zeid et al. (2009) ran simulations of a university campus, varying the representation of the buildings (i.e., by combining multiple buildings for some simulations). They concluded that a high level of building detail did not have a significant impact on mean flow and aerodynamic properties—suggesting that rather coarse parametrizations of building geometry are acceptable when using LES to develop urban canopy parametrizations for large-scale weather prediction models. However, turbulence properties were found to vary significantly with the level of building detail included in simulations, indicating that high-fidelity representations of urban geometry are necessary for understanding turbulence and dispersion.

3.5.2 Urban Dispersion and Scalar Transport

In addition to studying mean flow and turbulence properties, LES has also been employed to investigate urban air quality and dispersion. A significant number of these studies (Walton and Cheng 2002; Baker et al. 2004; Cai et al. 2008; Li et al. 2008, 2010; Michioka et al. 2014) consider the question of how a passive scalar (or pollutant) released in an urban street canyon is transported vertically and the following picture has emerged. When the wind direction is perpendicular to the street-canyon axis, a recirculation vortex forms in the street canyon, with its axis parallel to that of the street canyon. Secondary vortices may also form; this depends on the street-canyon aspect ratio $\mathcal{A} = HW^{-1}$ and thermal stratification. For neutral stratification with an aspect ratio of $\mathcal{A} \approx 1$, lower scalar concentrations are found on the

downstream wall of the street canyon, where vertical profiles are nearly constant. On the upstream wall, concentration peaks near the ground, and then decreases with height zH^{-1} (Walton and Cheng 2002). For a scalar released from an area source at ground level, the vertical flux of scalar at the canopy top ($\langle w'c' \rangle$) decreases with increasing canyon aspect ratio $\mathcal{A}$ (Cai et al. 2008). For street canyons with very high aspect ratio (e.g. $\mathcal{A} > 3$), multiple counter-rotating recirculation vortices form throughout the depth of the street canyon, and the vertical scalar flux at the canopy top is greatly diminished compared to the $\mathcal{A} \approx 1$ case (Li et al. 2008). Ground heating facilitates pollutant removal from the street canyon. In this case, vertical buoyancy forces modify the recirculation vortex within the canyon, leading to lower scalar concentrations within the canyon and larger values of $\langle w'c' \rangle$ at street-canyon top (Li et al. 2010).

Michioka et al. (2014) investigated the more realistic case of street canyons with finite length in the cross-stream direction, finding that as the length-to-height ratio LH^{-1} decreased, lateral dispersion (due to flow channeling between buildings) was enhanced, leading to decreased concentrations within the street canyon. Baker et al. (2004) considered the case of reactive scalars, namely NO and NO_2 emitted from a line source within a street canyon (modelling emissions from traffic), with background values of ozone (O_3). They found significant spatial variability in ozone within the street canyon, which has major implications for pedestrian exposure to pollutants.

Large-eddy simulation studies have also examined point-source scalar dispersion in idealized (cuboid arrays) or realistic urban canopies. Using an IBM, Tseng et al. (2006) simulated point-source scalar dispersion in downtown Baltimore, Maryland, presenting evidence of channeling of the scalar plume around buildings, and significant spatial and temporal variability of scalar concentration. Xie and Castro (2009) performed scalar dispersion simulations for central London (for the DAPPLE experiment location), finding reasonable agreement between LES and observations and significant flow channeling around buildings. In a follow-up study, Xie (2011) forced LES dispersion simulations for the DAPPLE site with realistic wind data, finding that this improved agreement between LES and observations; predicted scalar concentrations from LES were found to have a significant dependence on wind angle.

Philips et al. (2013) performed LES of point-source passive scalar dispersion over arrays of cuboids in order to investigate how urban geometry impacts scalar plume statistics. They found that staggered buildings increased lateral dispersion, whereas aligned buildings enhanced vertical dispersion. Plumes became narrower with increasing source height within the urban canopy. In addition, they found that the vertical plume spread σ_z, had similar behavior for all plumes several building heights downstream, but the lateral plume spread σ_y varied significantly depending on the source location and urban geometry (λ_p, λ_f, and whether buildings were staggered or aligned). In other recent work, Santos et al. (2019) used LES to investigate the ratio of peak to mean concentration in urban dispersion simulations; LES output was used to estimate the value of a power-law exponent in a model relating maximum to mean concentration. However, they found that results were somewhat sensitive to the choice of SGS model and grid spacing.

3.6 Large-Scale Spatial Heterogeneity

Landscape heterogeneities are intrinsically linked to locally elevated surface fluxes of momentum, heat, humidity, and other quantities including pollen and dust. Such surface fluxes are a product of land–atmosphere interactions affecting the hydrologic cycle, and local heterogeneities create microclimates that profoundly alter the existence of surface

layer-like conditions. Herein, we adopt the contemporary structural paradigm of ASL turbulence, wherein a hierarchy of attached eddies (as per MOST) are structurally autonomous but dynamically modulated by the passage of yet-larger structures meandering within the flow (Lemone 1976; Hutchins and Marusic 2007; Salesky and Anderson 2018). The limiting extent for attached eddies, $\lambda_{a,1} \sim \delta$, while the limiting extent for the larger-scale structures is $\lambda_{a,2} \sim 10^1\delta \sim 10^1\lambda_{a,1}$. In this context, spatial landscape heterogeneities can themselves be decomposed based on the characteristic length of the heterogeneities, λ_l. For $\lambda_l\delta^{-1} < 1$ and $\lambda_l\delta^{-1} > 1$, the landscape heterogeneity is small- and large-scale, respectively. In the case of the former, individual roughness sublayer processes are homogenenized within the flow; for the latter, flow heterogeneities are persistent over the depth of the flow. The remainder of this discussion is devoted to the latter.

Landscape heterogeneities occur via spatial variation in aerodynamic, thermal, and moisture conditions. For simplicity, these different landscape conditions are discussed separately starting with the use of LES to determine large-scale response to canonical variation in aerodynamic conditions. For the scenario in which the prevailing wind direction is aligned to encounter a streamwise step-change in surface roughness, from z_{0-} to z_{0+} (where z_{0-} to z_{0+} are surface roughness lengths), a significant body of knowledge exists on the resulting flow field. If $z_{0+} > z_{0-}$ (the smooth-to-rough transition), an internal (momentum) boundary-layer (IBL), depth δ_i, forms at the transition and grows in thickness downwind of the transition (Brutsaert 1982). Dimensional analysis (Garratt 1990) has indicated that δ_i is dependent on downwind position, x, and z_{0+} as first expressed by the Wood (1981) model,

$$\delta_i\,(x, z_{0+}) = C z_{0+} \left(\frac{x}{z_{0+}}\right)^n, \tag{19}$$

where field and experimental data generally have indicated $C = 0.28$ and $n \approx 0.8$ (Antonia and Luxton 1971). Further, the abrupt transition in roughness results in an abrupt rise in surface stress, and elevated production of turbulence in the fluid immediately above and downwind of the transition (Antonia and Luxton 1971; Bou-Zeid et al. 2004). These effects introduce mean flow disturbances, which change the boundary layer and prevent reduction of the momentum transport equations under the horizontal statistical homogeneity assumption, $\partial\langle\tilde{u}_i\rangle_{xy}/\partial x = \partial\langle\tilde{u}_i\rangle_{xy}/\partial y = \langle\tilde{v}\rangle_{xy} = \langle\tilde{w}\rangle_{xy} = 0$ for i =1–3 (Belcher et al. 2012). Bou-Zeid et al. (2004) ran a comprehensive LES parametric study to evaluate the effects of changing the aerodynamic roughness length, and the width of high-roughness streamwise heterogeneous "strips", while Bou-Zeid et al. (2007) considered yet more complex scenarios of topographies composed of squares of varying roughness. These studies found that the average momentum fluxes are well characterized by an effective aerodynamic roughness length $z_{o,e}$.

The influence of spanwise-varying surface stress has gained substantial interest in recent years, although prior efforts have been directed towards hydraulic engineering applications (open channel flows) or to fundamental wall turbulence studies. Studies have shown that there is a high degree of spanwise heterogeneity in the mean flow when the surface roughness features a prominent spanwise heterogeneity (Nugroho et al. 2013; Willingham et al. 2013; Anderson et al. 2015; Yang and Anderson 2017; Hwang and Lee 2018; Anderson 2019b). This research has revealed that elevated drag across "rough" regions induces spatial heterogeneities in the Reynolds (turbulent) stresses (Tennekes and Lumley 1972; Pope 2000). It has been shown (Anderson et al. 2015) that a turbulence production–dissipation imbalance above the "rough" zones necessitates a downwelling of momentum from aloft (Hinze 1967), which thus necessitates a lateral outflow and corresponding upwelling across the "smooth" areas. More recently, intermediate cases wherein the landscape heterogeneity is aligned oblique to the main transport direction have been considered (Anderson 2019a).

Research examining ABL response to thermal and moisture heterogeneities at the land surface has largely focused on the CBL using either idealized or data driven patterns of surface sensible heat flux, potential temperature, surface moisture, or some combination. Early studies used one- or two- dimensional sinusoidal patterns to examine how heterogeneity wavelength (λ_l) and amplitude affected CBL fluxes (Hadfield et al. 1992; Shen and Leclerc 1995; Avissar and Schmidt 1998; Baidya Roy and Avissar 2000). These studies established that only wavelengths $\lambda_l > \delta$ had an appreciable impact on horizontally averaged vertical fluxes and boundary-layer turbulence statistics. For all values of λ_l, stronger background winds decreased the impact of heterogeneity and all studies observed turbulence enhancements over the flux maxima, including enhanced updrafts and enhanced values of the velocity and potential temperature variances near the surface. Which velocity components were affected the most depended on if the heterogeneity pattern was one or two dimensional (Shen and Leclerc 1995; Courault et al. 2007). The primary explanation for observed flux and variance enhancements was secondary circulations resulting from localized pressure gradients created by horizontal temperature differences. With stronger background winds, these pressure gradients wash out. As the strength of the organized circulations increases, they were found to countervail the random patterns observed in the homogeneous CBL (Avissar and Schmidt 1998, see Sect. 3.1.1 for homogeneous CBL dynamics). Importantly, the signature of homogeneous CBL turbulence is not eliminated by this process, it is simply hidden in time-averaged fields (Baidya Roy and Avissar 2000). What constitutes a strong background wind depends on the orientation of the flow with respect to the heterogeneity patterns. Raasch and Harbusch (2001) reported measurable impacts, even under strong background flow, with checkerboard heterogeneity when the flow is aligned with the diagonals of the surface flux pattern. Furthermore, Courault et al. (2007) reported that spanwise homogeneous strips had an enhanced impact compared to checkerboard type patterns and that using a model that couples the surface state variables to the ABL appears to dampen the signature of surface heterogeneity by lessening flux contrasts.

Natural patterns derived from aircraft and satellite based remotely sensed surface conditions have also been explored. One of the first was Hechtel et al. (1990) who used surface sensible and latent heat flux heterogeneity distributions chosen to match the spectra of measured surface temperature distributions taken from aircraft flight transects. The simulations had modest agreement with measurements and did not differ significantly from an equivalent homogeneous run. A few possible explanations for the lack of sensitivity were given: poor simulation characteristics (SGS models, grid resolution), presence of a background flow, and the small value of λ_l (only slightly larger than the grid scale). Various levels of coupling between the land surface and the ABL through either a two-source model (Albertson et al. 2001; Kustas and Albertson 2003), or a full land-surface model (Huang and Margulis 2010) have also been explored. These simulations generally agreed with field measurements supporting the idealized study conclusions that heterogeneity length scales smaller than δ have minimal impact on CBL fluxes. Kustas and Albertson (2003) examined the impact of a surface temperature contrast with their model and found that enhanced contrast did not appreciably affect horizontally averaged fluxes. They surmised that this was a result of the feedback between secondary circulations and surface fluxes allowed by coupled models in agreement with more idealized studies (Courault et al. 2007).

In contrast to the neutral heterogeneous ABL discussed above, in the heterogeneous CBL the impact of heterogeneity is found to propagate up through the ASL for sufficiently large λ_l with both idealized and realistic heterogeneity patterns (Baidya Roy and Avissar 2000; Huang and Margulis 2010; Maronga and Raasch 2013). This invalidates the concept of a "blending-height" used in mosaic, tile, and many bulk methods that researchers have found

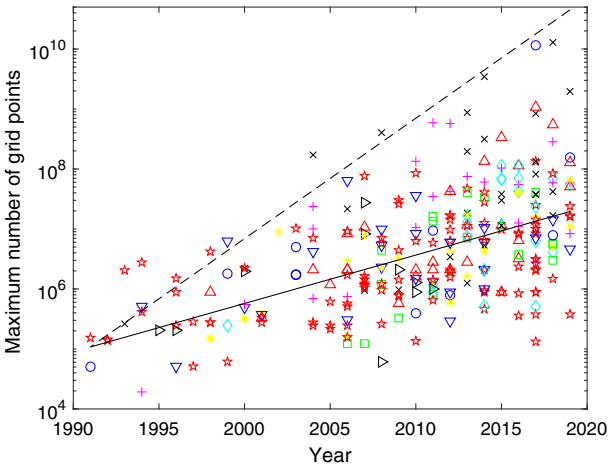

Fig. 4 Maximum number of grid points used in LES published in *BLM* since 1990. The solid line corresponds to a best fit power law of $2^{0.27}$ and the dashed line to the theoretical value of $2^{0.67}$

to be successful in heterogeneous neutral and stably stratified ABLs (e.g., Bou-Zeid et al. 2004; Miller and Stoll 2013).

4 Future of LES

4.1 Simulation Scaling Trends

The history and usage of LES for ABL applications is tied to the development of modern computing. One measure researchers have used to link computational physics to advancements in computing is to examine the scaling relationship between the maximum number of grid points used in a simulation and the years since activities commenced (Voller and Porté-Agel 2002; Bou-Zeid 2015). We performed this analysis for all the identifiable LES papers published in *BLM* (Fig. 4). Our analysis was restricted to *BLM* so that it would be representative of research efforts in the ABL community and the trajectory of work published in the journal. Articles that used LES data from other publications were not included to remove any biases in timing that might emerge from data reuse. Additionally, articles in which the maximum number of grid points could not be readily identified were skipped (see the Online Resources for DOI information on all articles used in Fig. 4). Although the first simulations were run in the 1970s, scaling fits to Moore's law were done starting from 1990 when the trend in the number of simulations per year increased. Fits prior to this produce highly variable results due to the extremely low number of samples per year.

It is immediately evident from Fig. 4 that, on average, LES-based articles published in *BLM* do not follow Moore's law. While it is questionable if Moore's law will hold into the future, it has been approximately valid for the range of years we studied (Khan et al. 2018). Interestingly, the scaling exponent (0.27) is close to that found for DNS-based articles from *JFM* (Bou-Zeid 2015). Although the best-fit trend does not follow Moore's law, there are simulations that do, indicating it was possible during the study period.

Table 1 Number of articles identified for each country or region group and the corresponding symbol used in Fig. 4

Countries	Number of articles	Symbol
Australia, Malaysia, New Zealand, Singapore, Korea	12	◯
China	17	□
Japan	23	+
Belgium, Croatia, Denmark, Finland, Italy, Norway, Poland, Portugal, Spain, Sweden	28	△
Netherlands, Switzerland	21	◊
Germany	28	x
France	20	*
England	25	▽
Brazil, Canada	10	▷
United States	104	⋆

Of interest is why the best-fit trend is well below Moore's law. One possible explanation is that LES users frequently choose to run simulations using fewer grid points out of convenience. This could be out of a desire to use available desktop computing resource instead of shared high-performance computing (HPC) systems, or to avoid the hassle associated with the analysis of the extremely large datasets that result from running biggest-possible simulations. The similar scaling exponent to that found for DNS suggests otherwise if it is assumed that researchers are not purposefully targeting lower Reynolds numbers than they could achieve because it is nearly always desirable in a DNS study to maximize Reynolds number. An alternative explanation is that ABL LES users frequently run ensembles to examine a particular hypothesis (e.g., sensitivity of a physical process to large-scale forcing) limiting their available maximum number of grid points. To explore this, the number of ensemble members at the maximum number of grid points was recorded for each paper as well as the total number of prognostic variables used in the simulation to examine if physical complexity contributes to the decreased scaling exponent. The scaling exponent calculated from the product of the maximum number of grid points, the number of prognostic variables, and the number of ensemble members is only slightly larger (0.29) than that for only the maximum number of grid points a strong counter to this explanation.

A third possibility is that the lower exponent is indicative of resource limitations. Researchers would run with more grid points but they do not have access to the required HPC infrastructure or, they do not have the required resources or experience to improve their software infrastructure to take full advantage of available HPC. One testable hypothesis related to this is that if resource limitations have some explanatory power it would manifest through different trends in different countries as a result of disparities in funding levels and or the effectiveness of different funding systems (e.g., Sandström and Van den Besselaar 2018). Country of origin was assumed to be the country of the corresponding author. To enable trend detection, countries without sufficient numbers of papers attributed to them were grouped. The grouping was loosely done by region under the assumption that resources were more likely than not to be similar in a geographic region (Table 4).

When the scaling plot is broken down by country, some trends can be discerned. First, it is evident that the majority of the simulations since 2004 that achieve the theoretical scaling have an origin in Germany. This is only a short time after the introduction of the parallelized LES model (PALM, Raasch and Schröter 2001). A second observation is that although many of the initial simulations that are close to the theoretical line are from groups in the United States and England, after 2007 we see a reduction in the maximum number of grid points from these two countries. Because simulations from only one journal are included in the analysis, it is difficult to take this as more than an indicator that further inquiry is merited.

4.2 The *Terra-Incognita* in Large-Eddy Simulations

A fundamental pillar of LES is the filtering operation at scale Δ that enables partial resolution of turbulent eddies, and requires modelling of the smaller unresolved ones (Lilly 1967). If Δ is of similar order to the Kolmogorov scale, the limit of DNS is reached. Alternatively, if filtering takes place beyond the inertial regime, at scales larger or similar to the turbulence integral length scale (l_i) the limit of RANS is approached. When the former limit is asymptotically approached, the corresponding contribution of the SGS terms are small, especially in regions far from solid objects, or interfaces. As a result, the progressive evolution of LES towards DNS only hinges on the continuous development of faster and more capable computers (e.g., Fig. 4). Much to the contrary, in the latter limit where filtering occurs at very large scales, i.e. in the vicinity of the local turbulence integral scale ($l_i/\Delta \sim 1$), the so-called '*Terra-Incognita*' region or 'grey zone' is reached (Wyngaard 2004; Honnert et al. 2020), where the conceptual basis on which current LES SGS modelling stands crumbles. This challenging limit is traditionally the fringe region between the realm of numerical weather prediction (based on a RANS approach) and LES, and thus happens to be the region where most publications in ABL flows are developed.

The backbone of LES is K-41, which predicts the existence of an inertial regime where TKE is not generated, nor destroyed, but simply transferred through an eddy cascade. This a priori simplistic transfer of energy from bigger to smaller turbulent eddies provides a window of opportunity for models, which besides the traditional physical constraints of Galilean mechanics (Pope 2000), only have to ensure the appropriate transfer of energy. The challenge arises when filtering occurs at scales either too close to the inertial limit, or beyond, given that flow dynamics in this region can be dominated by strong non-linear interactions between the mean flow and turbulence. More specifically, at these large scales TKE is no longer simply transferred, but turbulence can actively interact with the mean flow, potentially leading to an additional generation or destruction of TKE. This additional non-linear interaction will further dictate the extent of the TKE's inertial regime. Furthermore, at these large scales there can also exist a backscatter of TKE from the turbulent eddies into the mean flow, which is not well predicted by K-41's theory, and hence missed in most SGS models. Therefore, the term of '*Terra-Incognita*' introduced in Wyngaard (2004), refers to the limit $l_i/\Delta \sim 1$, where neither LES nor mesoscale models were designed to operate. This limit represents an important challenge in developing multi-resolution models than can dynamically evolve from an LES to a RANS approach, as it is desired in most modelling of atmospheric flows and the theoretical limit of the '*Terra-Incognita*', is not a static limit to be addressed by adjusting the numerical resolution of the computational model, but instead should be considered through the glasses of a dynamical system. This is because a flow that can a priori be properly resolved, can progressively evolve as a result of external forcings towards the '*Terra-Incognita*' limit (Heerwaarden et al. 2014; Margairaz et al. 2020a, b). For example, consider a turbulent flow

with initial characteristic l_i that is being integrated with a fixed RANS grid resolution Δ such that $l_i/\Delta << 1$. At a later stage, due to external surface complexities (e.g. heterogeneous surface heating, changes in roughness, etc.), large-flow perturbations can develop such that now $l_i/\Delta \sim 1$. While initially the flow was well captured with the RANS approach, at the later stage this would fail to appropriately represent the flow physics because the simulation entered the '*Terra-Incognita*' region. A similar argument can be observed from the LES reference frame, e.g. consider a case where initially $l_i/\Delta >> 1$, the simulation then evolves towards a scenario where $l_i/\Delta \sim 1$ as a result of a reduction in l_i. This is the case for example in transitional boundary layers, going from unstable to stable stratification, where submeso motions can play a very important role (Sun et al. 2004; Mahrt and Thomas 2016).

At present the limitation of LES for poorly resolved large scales is the fact that there exists no theory that can universally predict the bijective interaction between the mean flow and unresolved, energy-containing eddies since this is case-to-case dependent, as expressed by the a priori neglected non-linear terms in the tendency equation for the mean shear stress in almost all models (Wyngaard 2004). Despite these challenges, researchers continue to use LES as a tool to develop and evaluate scale-aware parameterization schemes that can be applicable to weather models at grey-zone resolutions (Shin and Hong 2015; Shin and Dudhia 2016; Margairaz et al. 2020a). Nonetheless, the transition from RANS to LES simulations in an accurate, physics-based approach, remains a research chimera with the promise of great-gain and high-reward.

4.3 What is Next?

Over the last 50 years, the LES technique has gone from an emerging computational methodology to one of the major ways that researchers study the ABL. From its original roots studying simple channel flows and CBLs (Deardorff 1970a, 1972a), LES now covers all the primary application areas that ABL researchers explore. The technique itself has matured through a strong focus on theory, model development, and validation studies to the point where researchers trust it to provide insight into a wide range of turbulent phenomena in the ABL.

We surveyed six application areas where LES has been extensively applied to understand the performance of the technique and to study the physics of turbulent transport and its impact on the application of interest. These areas include the convective boundary layer, the stable boundary layer, transitional boundary layers, plant canopy flows, urban flows and dispersion, and land-surface heterogeneity. In each area, a common theme can be identified. Applications begin by adding any additional physics missing from prior studies and then they examine the validity of the LES technique and refine deficient models. Although this cycle of development does not ever completely end, after it is mature researchers in a given application area move towards ever more complex case studies aimed at increasing the realism of simulations. The increasing complexity has allowed researchers to widen their understanding of ABL fluxes of momentum and scalars and turn the LES technique into a tool that complements inquires using theory and laboratory and field experiments.

When we think about what the next frontiers are for ABL LES we can identify a few areas. One is further model development, including SGS models when energy containing length scales are poorly resolved in the '*Terra-Incognita*' (e.g., strong stratification without extreme resolution) and especially for surface boundary conditions. In nearly all flows with the exception of dense plant canopies, boundary conditions at the land (or building) surface play a critical role in the exchange of momentum, heat, and moisture between the land

surface and the atmosphere and ultimately in ABL dynamics. Even though this is well known, most modeling efforts use equilibrium models (Eq. 9) with a poor description of the land surface. Efforts to develop better models have been progressing including those that attempt to improve the representation of unresolved features (Anderson and Meneveau 2011) and non-equilibrium models that use the integral form of the boundary-layer equations (Yang et al. 2015). Yet general models that can address the wide range of surface and atmospheric conditions found in the ABL are still needed. This includes the impacts of local advection, stratification, and slope. In particular, proper LES surface boundary conditions for slope flows basically do not exist.

Another frontier is the continued march towards more realistic forcing, domains, boundary conditions, and physical descriptions. As computing power has increased, researchers in all the application areas continue to push towards conditions that more closely match those observed in the ABL. This has been enabled by the continued growth in computational power (e.g., Fig. 4), a need for better knowledge of the physics of the ABL, and a desire to move towards predictive LES. Researchers have already used the available computational power to address questions that are intractable in any other way. Although not reviewed here, an early example comes from the cloud modeling community where very large domain simulations have enabled the study of deep tropical convection and its impact on cloud formation, a critical component toward improving the representation of clouds in global climate models (Khairoutdinov et al. 2009). More recently, (Dipankar et al. 2015; Heinze et al. 2017) have explored the ability of LES to resolve convection and cloud processes at a spatial extent that covered all of Germany. Although the model was coarse for LES and used a simple SGS model, comparisons to data were satisfactory. Other researchers have shown that it is not only possible to simulate large domains but that long time integrations can also be done (Schalkwijk et al. 2016).

These efforts and others indicate that a path towards predictive LES of near surface processes is possible. Using the fits depicted in Fig. 4, we can estimate when we might be able to carry out LES with sufficient resolution to resolve diurnal ABL processes (e.g., not just convection) and large enough extent to be relevant to mesoscale weather. Based on work examining moderately statified SBLs (Beare et al. 2006; Sullivan et al. 2016) a grid resolution $\Delta \approx 10$ m is sufficient to nominally resolve terrain and SBL features. If we further assume a vertical domain extent of 5 km would start to capture mesoscale weather features, numerical codes that achieve scaling at the theoretical limit would be able to simulate a horizontal domain the size of a mid-sized state in the western United States (e.g., Utah) or a mid sized country in Europe (e.g., the United Kingdom) in around 2026. While this is encouraging, when the average scaling is used the soonest you would expect similar simulation would be 2078. If we extend to horizontal domains on the order of the entire United States (or approximately Europe), this is at best possible in 2035 and following the average scaling in 2099.

Many barriers still exist to LES becoming a tool that can be used to study the full range of ABL physics and even move on to becoming a predictive modelling tool. These include improved models and boundary conditions that can adapt to the wide range of possible surface conditions, continued improvements to lateral coupling with coarser scale models (e.g., Muñoz-EsTarza et al. 2014; Rai et al. 2019), and more work to generate the knowledge and understanding of the '*Terra-Incognita*' region, so coupling of multi-resolution models becomes physics based instead of current ad-hoc approaches. In addition, higher resolution of ABL processes and land–atmosphere coupling will require continued improvements to our description of the land surface itself. Advancements in thermal and lidar remote sensing are hopeful paths to this (e.g., Kustas and Anderson 2009; Liu et al. 2017) but significant work

is still required to turn the information these techniques provide into the surface descriptions that simulations need. Lastly, for these goals to be broadly met by researchers more simulation codes will need software infrastructure upgrades and ABL researchers will need continued and improved access to high performance computing hardware.

Acknowledgements This research was supported by the National Science Foundation Grants AGS-1660367 (R. Stoll and J. Gibbs) and PDM-1649067 and PDM-1712538 (M. Calaf) and the NOAA/Office of Oceanic and Atmospheric Research under NOAA–University of Oklahoma Cooperative Agreement NA11OAR4320072, U.S. Department of Commerce (J. Gibbs).

References

Ackerman AS, vanZanten MC, Stevens B, Savic-Jovcic V, Bretherton CS, Chlond A, Golaz JC, Jiang H, Khairoutdinov M, Krueger SK, Lewellen DC, Lock A, Moeng CH, Nakamura K, Petters MD, Snider JR, Weinbrecht S, Zulauf M (2009) Large-eddy simulations of a drizzling, stratocumulus-topped marine boundary layer. Mon Weather Rev 137(3):1083–1110. https://doi.org/10.1175/2008MWR2582.1

Adrian RJ, Meinhart CD, Tomkins CD (2000) Vortex organization in the outer region of the turbulent boundary layer. J Fluid Mech 422:1–54

Albertson JD, Kustas WP, Scanlon TM (2001) Large-eddy simulation over heterogeneous terrain with remotely sensed land surface conditions. Water Resour Res 37(7):1939–1953

Anderson R, Meneveau C (1999) Effects of the similarity model in finite-difference LES of isotropic turbulence using a Lagrangian dynamic mixed model. Flow Turbul Combust 62(3):201–225

Anderson W (2012) An immersed boundary method wall model for high-Reynolds number channel flow over complex topography. Int J Numer Methods Fluids 71:1588–1608

Anderson W (2019a) A15-1-15. J Fluid Mech 869:27–84

Anderson W (2019b) Non-periodic phase-space trajectories of roughness-driven secondary flows in high-re_τ boundary layers and channels. J Fluid Mech 869:27–84

Anderson W, Meneveau C (2010) A large-eddy simulation model for boundary-layer flow over surfaces with horizontally resolved but vertically unresolved roughness elements. Boundary-Layer Meteorol 137:397–415

Anderson W, Meneveau C (2011) Dynamic roughness model for large-eddy simulation of turbulent flow over multiscale, fractal-like rough surfaces. J Fluid Mech 679:288–314

Anderson W, Barros J, Christensen K, Awasthi A (2015) Numerical and experimental study of mechanisms responsible for turbulent secondary flows in boundary layer flows over spanwise heterogeneous roughness. J Fluid Mech 768:316–347

Andren A (1995) The structure of stably stratified atmospheric boundary layers: a large-eddy simulation study. Q J R Meteorol Soc 121(525):961–985

Andren A, Brown AR, Mason PJ, Graf J, Schumann U, Moeng CH, Nieuwstadt FT (1994) Large-eddy simulation of a neutrally stratified boundary layer: a comparison of four computer codes. Q J R Meteorol Soc 120(520):1457–1484

Antonia R, Luxton R (1971) The response of a turbulent boundary layer to a step change in surface roughness part i. Smooth to rough. J Fluid Mech 48:721–761

Armenio V, Sarkar S (2002) An investigation of stably stratified turbulent channel flow using large-eddy simulation. J Fluid Mech 459:1–42

Aumond P, Masson V, Lac C, Gauvreau B, Dupont S, Berengier M (2013) Including the drag effects of canopies: real case large-eddy simulation studies. Boundary-Layer Meteorol 146(1):65–80

Avissar R, Schmidt T (1998) An evaluation of the scale at which ground-surface heat flux patchiness affects the convective boundary layer using large-eddy simulations. J Atmos Sci 55(16):2666–2689. https://doi.org/10.1175/1520-0469(1998)055<2666:AEOTSA>2.0.CO;2

Ayotte KW, Sullivan PP, Andren A, Doney SC, Holtslag AA, Large WG, McWilliams JC, Moeng CH, Otte MJ, Tribbia JJ et al (1996) An evaluation of neutral and convective planetary boundary-layer parameterizations relative to large eddy simulations. Boundary-Layer Meteorol 79(1–2):131–175

Baidya Roy S, Avissar R (2000) Scales of response of the convective boundary layer to land-surface heterogeneity. Geophys Res Lett 27(4):533–536

Bailey BN, Stoll R (2013) Turbulence in sparse, organized vegetative canopies: a large-eddy simulation study. Boundary-Layer Meteorol 147:369–400. https://doi.org/10.1007/s10546-012-9796-4

Bailey BN, Stoll R (2016) The creation and evolution of coherent structures in plant canopy flows and their role in turbulent transport. J Fluid Mech 789:425–460
Bailey BN, Stoll R, Pardyjak ER, Mahaffee WF (2014) Effect of vegetative canopy architecture on vertical transport of massless particles. Atmos Environ 95:480–489
Baker J, Walker HL, Cai X (2004) A study of the dispersion and transport of reactive pollutants in and above street canyons—a large eddy simulation. Atmos Environ 38(39):6883–6892
Bao J, Chow F, Lundquist K (2018) Large-eddy simulation over complex terrain using an improved immersed boundary method in the weather research and forecasting mode. Mon Weather Rev 146:2781–2797
Bardina J, Ferziger J, Reynolds W (1980) Improved subgrid-scale models for large-eddy simulation. In: 13th Fluid and Plasma Dynamics Conference, pp 1–9. https://doi.org/10.2514/6.1980-1357
Basu S, Lacser A (2017) A cautionary note on the use of Monin–Obukhov similarity theory in very high-resolution large-eddy simulations. Boundary-Layer Meteorol 163(2):351–355
Basu S, Porté-agel F, Foufoula-Georgiou E, Vinuesa JF, Pahlow M (2006) Revisiting the local scaling hypothesis in stably stratified atmospheric boundary-layer turbulence: an integration of field and laboratory measurements with large-eddy simulations. Boundary-Layer Meteorol 119(3):473–500. https://doi.org/10.1007/s10546-005-9036-2
Basu S, Holtslag AA, Van De Wiel BJ, Moene AF, Steeneveld GJ (2008a) An inconvenient truth about using sensible heat flux as a surface boundary condition in models under stably stratified regimes. Acta Geophys 56(1):88–99
Basu S, Vinuesa JF, Swift A (2008b) Dynamic LES modeling of a diurnal cycle. J Appl Meteorol Climatol 47(4):1156–1174
Beare RJ (2008) The role of shear in the morning transition boundary layer. Boundary-Layer Meteorol 129(3):395–410
Beare RJ, Macvean MK, Holtslag AA, Cuxart J, Esau I, Golaz JC, Jimenez MA, Khairoutdinov M, Kosovic B, Lewellen D, Lund TS, Lundquist JK, Mccabe A, Moene AF, Noh Y, Raasch S, Sullivan P (2006) An intercomparison of large-eddy simulations of the stable boundary layer. Boundary-Layer Meteorol 118(2):247–272
Belcher S, Harman I, Finnigan J (2012) The wind in the willows: flows in forest canopies in complex terrain. Annu Rev Fluid Mech 44:479–504
Bohrer G, Katul GG, Walko RL, Avissar R (2009) Exploring the effects of microscale structural heterogeneity of forest canopies using large-eddy simulations. Boundary-Layer Meteorol 132(3):351–382
Boppana V, Xie ZT, Castro IP (2010) Large-eddy simulation of dispersion from surface sources in arrays of obstacles. Boundary-Layer Meteorol 135(3):433–454
Boppana V, Xie ZT, Castro IP (2014) Thermal stratification effects on flow over a generic urban canopy. Boundary-Layer Meteorol 153(1):141–162
Bou-Zeid E (2015) Challenging the large eddy simulation technique with advanced a posteriori tests. J Fluid Mech 764:1–4
Bou-Zeid E, Meneveau C, Parlange M (2004) Large-eddy simulation of neutral atmospheric boundary layer flow over heterogeneous surfaces: blending height and effective surface roughness. Water Resour Res 40(W02):505
Bou-Zeid E, Meneveau C, Parlange M (2005) A scale-dependent Lagrangian dynamic model for large eddy simulation of complex turbulent flows. Phys Fluids 17(2):025,105. https://doi.org/10.1063/1.1839152
Bou-Zeid E, Parlange M, Meneveau C (2007) On the parameterization of surface roughness at regional scales. J Atmos Sci 64:216–227
Bou-Zeid E, Overney J, Rogers BD, Parlange MB (2009) The effects of building representation and clustering in large-eddy simulations of flows in urban canopies. Boundary-Layer Meteorol 132(3):415–436
Boudreault LÉ, Dupont S, Bechmann A, Dellwik E (2017) How forest inhomogeneities affect the edge flow. Boundary-Layer Meteorol 162(3):375–400
Brown AR, Derbyshire S, Mason PJ (1994) Large-eddy simulation of stable atmospheric boundary layers with a revised stochastic subgrid model. Q J R Meteorol Soc 120(520):1485–1512
Brutsaert W (1982) Evaporation into the atmosphere. Kluwer, Norwell
Cai XM (2012) Effects of wall heating on flow characteristics in a street canyon. Boundary-Layer Meteorol 142(3):443–467
Cai XM, Barlow J, Belcher S (2008) Dispersion and transfer of passive scalars in and above street canyons–large-eddy simulations. Atmos Environ 42(23):5885–5895
Carper MA, Porté-Agel F (2004) The role of coherent structures in subfilter-scale dissipation of turbulence measured in the atmospheric surface layer. J Turbul 5:32–32
Carper MA, Porté-Agel F (2008) Subfilter-scale fluxes over a surface roughness transition. Part ii: a priori study of large-eddy simulation models. Boundary-Layer Meteorol 127(1):73–95

Cassiani M, Katul G, Albertson J (2008) The effects of canopy leaf area index on airflow across forest edges: large-eddy simulation and analytical results. Boundary-Layer Meteorol 126(3):433–460
Castagnera K, Cheng D, Fatoohi R, Hook E, Kramer B, Manning C, Musch J, Niggley C, Saphir W, Sheppard D et al (1994) Clustered workstations and their potential role as high speed compute processors. NAS Computational Services Technical Report RNS-94-003, NAS Systems Division, NASA Ames Research Center
Castro IP (2017) Are urban-canopy velocity profiles exponential? Boundary-Layer Meteorol 164(3):337–351
Chester S, Meneveau C, Parlange M (2007) Modelling of turbulent flow over fractal trees with renormalized numerical simulation. J Comp Phys 225:427–448
Chow FK, Street RL, Xue M, Ferziger JH (2005) Explicit filtering and reconstruction turbulence modeling for large-eddy simulation of neutral boundary layer flow. J Atmos Sci 62(7):2058–2077
Clark T (1977) A small-scale dynamic model using terrain-following coordinate transformation. J Comp Phys 24:186–215
Colwell RP (2019) How we made the pentium processors. Nat Electron 2(2):83–84
Conzemius RJ, Fedorovich E (2006) Dynamics of sheared convective boundary layer entrainment. Part i: methodological background and large-eddy simulations. J Atmos Sci 63(4):1151–1178
Courault D, Drobinski P, Brunet Y, Lacarrere P, Talbot C (2007) Impact of surface heterogeneity on a buoyancy-driven convective boundary layer in light winds. Boundary-Layer Meteorol 124(3):383–403
Cui Z, Cai X, Baker J, C, (2004) Large-eddy simulation of turbulent flow in a street canyon. Q J R Meteorol Soc 130(599):1373–1394
Cuxart J, Holtslag AA, Beare RJ, Bazile E, Beljaars A, Cheng A, Conangla L, Ek M, Freedman F, Hamdi R, Kerstein H, Kitagawa G, Lenderink D, Lewellen J, Mailhot T, Mauritsen V, Perov G, Schayes GJ, Steeneveld GS, Taylor P, Weng W, Wunsch S, Xu KM (2006) Single-column model intercomparison for a stably stratified atmospheric boundary layer. Boundary-Layer Meteorol 118(2):273–303
Deardorff JW (1970a) A numerical study of three-dimensional turbulent channel flow at large reynolds numbers. J Fluid Mech 41(2):453–480. https://doi.org/10.1017/S0022112070000691
Deardorff JW (1970b) Preliminary results from numerical integrations of the unstable planetary boundary layer. J Atmos Sci 27(8):1209–1211
Deardorff JW (1971) On the magnitude of the subgrid scale eddy coefficient. J Comp Phys 7(1):120–133. https://doi.org/10.1016/0021-9991(71)90053-2
Deardorff JW (1972a) Numerical investigation of neutral and unstable planetary boundary layers. J Atmos Sci 29:91–115. https://doi.org/10.1175/1520-0469(1972)029<0091:nionau>2.0.co;2
Deardorff JW (1972b) Theoretical expression for the countergradient vertical heat flux. J Geophys Res 77(30):5900–5904
Deardorff JW (1973) The use of subgrid transport equations in a three-dimensional model of atmospheric turbulence. J Fluids Eng 95(3):429–438. https://doi.org/10.1115/1.3447047
Deardorff JW (1974a) Three-dimensional numerical study of the height and mean structure of a heated planetary boundary layer. Boundary-Layer Meteorol 7(1):81–106
Deardorff JW (1974b) Three-dimensional numerical study of turbulence in an entraining mixed layer. Boundary-Layer Meteorol 7(2):199–226
Deardorff JW (1980) Stratocumulus-capped mixed layers derived from a three-dimensional model. Boundary-Layer Meteorol 18:495–527. https://doi.org/10.1007/BF00119502
Dipankar A, Stevens B, Heinze R, Moseley C, Zängl G, Giorgetta M, Brdar S (2015) Large eddy simulation using the general circulation model ICON. J Adv Model Earth Syst 7(3):963–986
Dörnbrack A, Schumann U (1993) Numerical simulation of turbulent convective flow over wavy terrain. Boundary-Layer Meteorol 65(4):323–355. https://doi.org/10.1007/BF00707032
Dupont S, Brunet Y (2008) Edge flow and canopy structure: a large-eddy simulation study. Boundary-Layer Meteorol 126(1):51–71
Dupont S, Gosselin F, Py C, De Langre E, Hemon P, Brunet Y (2010) Modelling waving crops using large-eddy simulation: comparison with experiments and a linear stability analysis. J Fluid Mech 652:5–44
Dwyer MJ, Patton EG, Shaw RH (1997) Turbulent kinetic energy budgets from a large-eddy simulation of airflow above and within a forest canopy. Boundary-Layer Meteorol 84(1):23–43
Ebert EE, Schumann U, Stull RB (1989) Nonlocal turbulent mixing in the convective boundary layer evaluated from large-eddy simulation. J Atmos Sci 46(14):2178–2207
Fedorovich E, Conzemius R, Esau I, Chow FK, Lewellen D, Moeng CH, Sullivan P, Pino D, de Arellano JVG (2004) Entrainment into sheared convective boundary layers as predicted by different large eddy simulation codes. In: 16th Symposium on boundary layers and turbulence, Portland, ME. American Meteorological Society, p P4.7
Fenger J (1999) Urban air quality. Atmos Environ 33(29):4877–4900
Finnigan J (2000) Turbulence in plant canopies. Annu Rev Fluid Mech 32(1):519–571

Finnigan JJ, Shaw RH, Patton EG (2009) Turbulence structure above a vegetation canopy. J Fluid Mech 637:387–424
Fitzmaurice L, Shaw RH, Paw UKT, Patton EG (2004) Three-dimensional scalar microfront systems in a large-eddy simulation of vegetation canopy flow. Boundary-Layer Meteorol 112(1):107–127
Gal-Chen T, Sommerville R (1975) On the use of a coordinate transformation for the solution of the Navier–Stokes equations. J Comp Phys 17:209–228
Galmarini S, Beets C, Duynkerke PG, Vila-Guerau de Arellano J (1998) Stable nocturnal boundary layers: a comparison of one-dimensional and large-eddy simulation models. Boundary-Layer Meteorol 88(2):181–210
Gao W, Shaw RH, Paw UKT (1989) Observation of organized structure in turbulent flow within and above a forest canopy. Boundary-Layer Meteorol 47(1):349–377. https://doi.org/10.1007/BF00122339
Garratt J (1990) The internal boundary layer—a review. Boundary-Layer Meteorol 40:171–203
Garratt JR (1992) The atmospheric boundary layer. Cambridge University Press, Cambridge
Germano M, Piomelli U, Moin P, Cabot WH (1991) A dynamic subgrid-scale eddy viscosity model. Phys Fluids A 3(7):1760–1765. https://doi.org/10.1063/1.857955
Geurts BJ (2003) Elements of direct and large eddy simulation. RT Edwards, Inc, West Bundaberg
Ghosal S, Lund TS, Moin P, Akselvoll K (1995) A dynamic localization model for large-eddy simulation of turbulent flows. J Fluid Mech 286:229–255. https://doi.org/10.1017/S0022112095000711
Giacomini B, Giometto MG (2020) On the suitability of general-purpose finite-volume-based solvers for the simulation of atmospheric-boundary-layer flow. Geosci Model Dev Discuss. https://doi.org/10.5194/gmd-2020-84
Gibbs JA, Fedorovich E (2014a) Comparison of convective boundary layer velocity spectra retrieved from large-eddy-simulation and weather research and forecasting model data. J Appl Meteorol Climatol 53(377):394. https://doi.org/10.1175/jamc-d-13-033.1
Gibbs JA, Fedorovich E (2014b) Effects of temporal discretization on turbulence statistics and spectra in numerically simulated convective boundary layers. Boundary-Layer Meteorol 153(19):41. https://doi.org/10.1007/s10546-014-9936-0
Gibbs JA, Fedorovich E (2016) Sensitivity of turbulence statistics in the lower portion of a numerically simulated stable boundary layer to parameters of the Deardorff subgrid turbulence model. Q J R Meteorol Soc 142(698):2205–2213
Gibbs JA, Fedorovich E, Shapiro A (2015) Revisiting surface heat-flux and temperature boundary conditions in models of stably stratified boundary-layer flows. Boundary-Layer Meteorol 154(2):171–187
Giometto M, Christen A, Meneveau C, Fang J, Krafczyk M, Parlange M (2016) Spatial characteristics of roughness sublayer mean flow and turbulence over a realistic urban surface. Boundary-Layer Meteorol 160(3):425–452
Giometto MG, Christen A, Egli PE, Schmid M, Tooke R, Coops N, Parlange MB (2017) Effects of trees on mean wind, turbulence and momentum exchange within and above a real urban environment. Adv Water Resour 106:154–168
Grimmond C, Oke TR (1999) Aerodynamic properties of urban areas derived from analysis of surface form. J Appl Meteorol 38(9):1262–1292
Grinstein FF, Margolin LG, Rider WJ (2007) Implicit large eddy simulation, vol 10. Cambridge University Press, Cambridge
Gropp W, Lusk E, Doss N, Skjellum A (1996) A high-performance, portable implementation of the MPI message passing interface standard. Parallel Comput 22(6):789–828
Hadfield MG, Cotton WR, Pielke RA (1992) Large-eddy simulations of thermally forced circulations in the convective boundary layer. Part II: the effect of changes in wavelength and wind speed. Boundary-Layer Meteorol 58:307–327
Hanna S, Tehranian S, Carissimo B, Macdonald R, Lohner R (2002) Comparisons of model simulations with observations of mean flow and turbulence within simple obstacle arrays. Atmos Environ 36(32):5067–5079
Hayati AN, Stoll R, Pardyjak ER, Harman T, Kim J (2019) Comparative metrics for computational approaches in non-uniform street-canyon flows. Build Environ 158:16–27
Hechtel LM, Stul RB, Moeng CH (1990) The effects of nonhomogeneous surface fluxes on the convective boundary layer: a case study using large-eddy simulation. J Atmos Sci 47(14):1721–1741. https://doi.org/10.1175/1520-0469(1990)047<1721:TEONSF>2.0.CO;2
Heerwaarden CCv, Mellado JP, Lozar AD, (2014) Scaling laws for the heterogeneously heated free convective boundary layer. J Atmos Sci 71(11):3975–4000. https://doi.org/10.1175/jas-d-13-0383.1
Heinze R, Dipankar A, Henken CC, Moseley C, Sourdeval O, Trömel S, Xie X, Adamidis P, Ament F, Baars H et al (2017) Large-eddy simulations over Germany using ICON: a comprehensive evaluation. Q J R Meteorol Soc 143(702):69–100

Hildebrand PH, Ackerman B (1984) Urban effects on the convective boundary layer. J Atmos Sci 41(1):76–91
Hinze JO (1967) Secondary currents in wall turbulence. Phys Fluids 10(9):S122–S125. https://doi.org/10.1063/1.1762429
Holtslag A, Moeng CH (1991) Eddy diffusivity and countergradient transport in the convective atmospheric boundary layer. J Atmos Sci 48(14):1690–1698
Holtslag A, Svensson G, Baas P, Basu S, Beare B, Beljaars A, Bosveld F, Cuxart J, Lindvall J, Steeneveld G et al (2013) Stable atmospheric boundary layers and diurnal cycles: challenges for weather and climate models. Bull Am Meteorol Soc 94(11):1691–1706
Honnert R, Efstathiou GA, Beare RJ, Ito J, Lock A, Neggers R, Plant RS, Shin HH, Tomassini L, Zhou B (2020) The atmospheric boundary layer and the gray zone of turbulence: a critical review. J Geophys Res Atmos. https://doi.org/10.1029/2019jd030317
Huang HY, Margulis SA (2010) Evaluation of a fully coupled large-eddy simulation-land surface model and its diagnosis of land-atmosphere feedbacks. Water Resour Res 46(6):
Huang J, Bou-Zeid E (2013) Turbulence and vertical fluxes in the stable atmospheric boundary layer. Part i: a large-eddy simulation study. J Atmos Sci 70(6):1513–1527
Huang J, Lee X, Patton EG (2009) Dissimilarity of scalar transport in the convective boundary layer in inhomogeneous landscapes. Boundary-Layer Meteorol 130(3):327–345
Hutchins N, Marusic I (2007) Evidence of very long meandering features in the logarithmic region of turbulent boundary layers. J Fluid Mech 579:1–28
Hwang H, Lee J (2018) Secondary flows in turbulent boundary layers over longitudinal surface roughness. Phys Rev Fluids 3(014):608
Jeong J, Hussain F (1995) On the identification of a vortex. J Fluid Mech 285:69–94
Kanda M (2006) Large-eddy simulations on the effects of surface geometry of building arrays on turbulent organized structures. Boundary-Layer Meteorol 118(1):151–168
Kanda M, Hino M (1994) Organized structures in developing turbulent flow within and above a plant canopy, using a large eddy simulation. Boundary-Layer Meteorol 68(3):237–257
Kanda M, Inagaki A, Letzel MO, Raasch S, Watanabe T (2004a) LES study of the energy imbalance problem with eddy covariance fluxes. Boundary-Layer Meteorol 110(3):381–404
Kanda M, Moriwaki R, Kasamatsu F (2004b) Large-eddy simulation of turbulent organized structures within and above explicitly resolved cube arrays. Boundary-Layer Meteorol 112(2):343–368
Kanda M, Inagaki A, Miyamoto T, Gryschka M, Raasch S (2013) A new aerodynamic parametrization for real urban surfaces. Boundary-Layer Meteorol 148(2):357–377
Khairoutdinov MF, Krueger SK, Moeng CH, Bogenschutz PA, Randall DA (2009) Large-eddy simulation of maritime deep tropical convection. J Adv Model Earth Syst 1(4)
Khan HN, Hounshell DA, Fuchs ER (2018) Science and research policy at the end of Moore's law. Nat Electron 1(1):14–21
Khanna S, Brasseur JG (1997) Analysis of Monin–Obukhov similarity from large-eddy simulation. J Fluid Mech 345:251–286
Khanna S, Brasseur JG (1998) Three-dimensional buoyancy-and shear-induced local structure of the atmospheric boundary layer. J Atmos Sci 55(5):710–743
Kim SW, Park SU, Moeng CH (2003) Entrainment processes in the convective boundary layer with varying wind shear. Boundary-Layer Meteorol 108(2):221–245
Kolmogorov AN, Levin V, Hunt JCR, Phillips OM, Williams D (1991) The local structure of turbulence in incompressible viscous fluid for very large Reynolds numbers. Proc R Soc Lond A 434(1890):9–13. https://doi.org/10.1098/rspa.1991.0075
Kosović B, Curry JA (2000) A large eddy simulation study of a quasi-steady, stably stratified atmospheric boundary layer. J Atmos Sci 57(8):1052–1068
Kröniger K, De Roo F, Brugger P, Huq S, Banerjee T, Zinsser J, Rotenberg E, Yakir D, Rohatyn S, Mauder M (2018) Effect of secondary circulations on the surface-atmosphere exchange of energy at an isolated semi-arid forest. Boundary-Layer Meteorol 169(2):209–232
Kumar V, Kleissl J, Meneveau C, Parlange MB (2006) Large-eddy simulation of a diurnal cycle of the atmospheric boundary layer: Atmospheric stability and scaling issues. Water Resour Res 42(6)
Kumar V, Svensson G, Holtslag A, Meneveau C, Parlange MB (2010) Impact of surface flux formulations and geostrophic forcing on large-eddy simulations of diurnal atmospheric boundary layer flow. J Appl Meteorol Climatol 49(7):1496–1516
Kustas W, Anderson M (2009) Advances in thermal infrared remote sensing for land surface modeling. Agric For Meteorol 149(12):2071–2081
Kustas WP, Albertson JD (2003) Effects of surface temperature contrast on land-atmosphere exchange: a case study from Monsoon 90. Water Resour Res 39(6)

Lemone M (1976) Modulation of turbulence energy by longitudinal rolls in an unstable planetary boundary layer. J Atmos Sci 33(7):1308–1320
LeMone MA, Angevine WM, Bretherton CS, Chen F, Dudhia J, Fedorovich E, Katsaros KB, Lenschow DH, Mahrt L, Patton EG et al (2019) 100 years of progress in boundary layer meteorology. Meteorol Monogr 59:1–9
Leonard A (1974) Energy cascade in large-eddy simulations of turbulent fluid flows. In: Turbulent diffusion in environmental pollution, pp 237–248
Lesieur M, Métais O, Comte P (2005) Large-eddy simulations of turbulence. Cambridge University Press, Cambridge. https://doi.org/10.1017/CBO9780511755507
Li Q, Gentine P, Mellado JP, McColl KA (2018) Implications of nonlocal transport and conditionally averaged statistics on Monin–Obukhov similarity theory and Townsend's attached eddy hypothesis. J Atmos Sci 75(10):3403–3431
Li XX, Liu CH, Leung DY (2008) Large-eddy simulation of flow and pollutant dispersion in high-aspect-ratio urban street canyons with wall model. Boundary-Layer Meteorol 129(2):249–268
Li XX, Britter RE, Koh TY, Norford LK, Liu CH, Entekhabi D, Leung DY (2010) Large-eddy simulation of flow and pollutant transport in urban street canyons with ground heating. Boundary-Layer Meteorol 137(2):187–204
Lilly DK (1967) The representation of small-scale turbulence in numerical simulations. In: Proceedings IBM scientific computing symposium on environmental sciences, Yorktown Heights, NY, IBM form no. 320-1951, pp 195–209
Lilly DK (1992) A proposed modification of the Germano subgrid-scale closure method. Phys Fluids A 4(3):633–635. https://doi.org/10.1063/1.858280
Lilly DK (2000) The meteorological development of large eddy simulation. In: Kerr RM, Kimura Y (eds) IUTAM symposium on developments in geophysical turbulence. Fluid mechanics and its applications, Chap 2, vol 58. Springer, Dordrecht, pp 5–18
Liu L, Coops NC, Aven NW, Pang Y (2017) Mapping urban tree species using integrated airborne hyperspectral and LiDAR remote sensing data. Remote Sens Environ 200:170–182
Liu S, Meneveau C, Katz J (1994) On the properties of similarity subgrid-scale models as deduced from measurements in a turbulent jet. J Fluid Mech 275:83–119. https://doi.org/10.1017/S0022112094002296
Lu H, Rutland CJ, Smith LM (2008) A posteriori tests of one-equation LES modeling of rotating turbulence. Int J Mod Phys C 19(12):1949–1964
Macdonald R (2000) Modelling the mean velocity profile in the urban canopy layer. Boundary-Layer Meteorol 97(1):25–45
Mahaffee WF, Stoll R (2016) The ebb and flow of airborne pathogens: monitoring and use in disease management decisions. Phytopathology 106(5):420–431
Mahrt L (1999) Stratified atmospheric boundary layers. Boundary-Layer Meteorol 90(3):375–396
Mahrt L, Thomas C (2016) Surface stress with non-stationary weak winds and stable stratification. Boundary-Layer Meteorol 159(1):3–21
Margairaz F, Pardyjak ER, Calaf M (2020a) Surface thermal heterogeneities and the atmospheric boundary layer: the heterogeneity parameter. Boundary-Layer Meteorol 1–27. https://doi.org/10.1007/s10546-020-00544-7
Margairaz F, Pardyjak ER, Calaf M (2020b) Surface thermal heterogeneities and the atmospheric boundary layer: the relevance of dispersive fluxes. Boundary-Layer Meteorol. https://doi.org/10.1007/s10546-020-00509-w
Maronga B, Raasch S (2013) Large-eddy simulations of surface heterogeneity effects on the convective boundary layer during the LITFASS-2003 experiment. Boundary-Layer Meteorol 146(1):17–44
Mason P, Callen N (1986) On the magnitude of the subgrid-scale eddy coefficient in large-eddy simulations of turbulent channel flow. J Fluid Mech 162:439–462
Mason PJ (1989) Large-eddy simulation of the convective atmospheric boundary layer. J Atmos Sci 46(11):1492–1516
Mason PJ, Derbyshire SH (1990) Large-eddy simulation of the stably-stratified atmospheric boundary layer. Boundary-Layer Meteorol 53:117–162. https://doi.org/10.1007/BF00122467
Mason PJ, Thomson DJ (1992) Stochastic backscatter in large-eddy simulations of boundary layers. J Fluid Mech 242:51–78. https://doi.org/10.1017/S0022112092002271
Matheou G, Chung D (2014) Large-eddy simulation of stratified turbulence. Part ii: application of the stretched-vortex model to the atmospheric boundary layer. J Atmos Sci 71(12):4439–4460
Mellado JP (2017) Cloud-top entrainment in stratocumulus clouds. Annu Rev Fluid Mech 49:145–169
Mellor GL, Yamada T (1974) A hierarchy of turbulence closure models for planetary boundary layers. J Atmos Sci 31(7):1791–1806

Meneveau C, Katz J (2000) Scale-invariance and turbulence models for large-eddy simulation. Annu Rev Fluid Mech 32(1):1–32. https://doi.org/10.1146/annurev.fluid.32.1.1
Meneveau C, Lund TS, Cabot WH (1996) A Lagrangian dynamic subgrid-scale model of turbulence. J Fluid Mech 319:353–385. https://doi.org/10.1017/S0022112096007379
Métais O (1998) Large-eddy simulations of three-dimensional turbulent flows: geophysical applications. Springer, Dordrecht, pp 351–372
Michioka T, Takimoto H, Sato A (2014) Large-eddy simulation of pollutant removal from a three-dimensional street canyon. Boundary-Layer Meteorol 150(2):259–275
Miller NE, Stoll R (2013) Surface heterogeneity effects on regional-scale fluxes in the stable boundary layer: aerodynamic roughness length transitions. Boundary-Layer Meteorol 149(2):277–301
Mirocha J, Lundquist J, Kosović B (2010) Implementation of a nonlinear subfilter turbulence stress model for large-eddy simulation in the advanced research WRF model. Mon Weather Rev 138(11):4212–4228
Mirocha JD, Kosović B (2010) A large-eddy simulation study of the influence of subsidence on the stably stratified atmospheric boundary layer. Boundary-Layer Meteorol 134(1):1
Mittal R, Iaccarino G (2005) Immersed boundary methods. Annu Rev Fluid Mech 37:239–261
Moeng CH (1984) A large-eddy-simulation model for the study of planetary boundary-layer turbulence. J Atmos Sci 41(13):2052–2062. https://doi.org/10.1175/1520-0469(1984)041<2052:ALESMF>2.0.CO;2
Moeng CH, Sullivan PP (1994) A comparison of shear-and buoyancy-driven planetary boundary layer flows. J Atmos Sci 51(7):999–1022
Moeng CH, Wyngaard JC (1988) Spectral analysis of large-eddy simulations of the convective boundary layer. J Atmos Sci 45(23):3573–3587
Moeng CH, Wyngaard JC (1989) Evaluation of turbulent transport and dissipation closures in second-order modeling. J Atmos Sci 46(14):2311–2330. https://doi.org/10.1175/1520-0469(1989)046<2311:EOTTAD>2.0.CO;2
Moin P, Homsy G (2017) An appreciation of the life and work of William C. Reynolds (1933–2004). Annu Rev Fluid Mech 49(1):1–21. https://doi.org/10.1146/annurev-fluid-122414-034434
Moin P, Squires K, Cabot W, Lee S (1991) A dynamic subgrid-scale model for compressible turbulence and scalar transport. Phys Fluids A 3(11):2746–2757
Monin A, Obukhov A (1954) Turbulent mixing in the atmospheric surface layer. Tr Akad Nauk SSSR Geofiz Inst 24(151):163–187
Muñoz-EsTarza D, Kosović B, Mirocha J, van Beeck J (2014) Bridging the transition from mesoscale to microscale turbulence in numerical weather prediction models. Boundary-Layer Meteorol 153(3):409–440
Nazarian N, Martilli A, Kleissl J (2018) Impacts of realistic urban heating, Part i: spatial variability of mean flow, turbulent exchange and pollutant dispersion. Boundary-Layer Meteorol 166(3):367–393
Nieuwstadt F, Brost R (1986) The decay of convective turbulence. J Atmos Sci 43(6):532–546
Nieuwstadt FT (1984) The turbulent structure of the stable, nocturnal boundary layer. J Atmos Sci 41(14):2202–2216
Nieuwstadt FT, Mason PJ, Moeng CH, Schumann U (1993) Large-eddy simulation of the convective boundary layer: a comparison of four computer codes. In: Turbulent shear flows, vol 8. Springer, Berlin, pp 343–367
Niyogi D, Pyle P, Lei M, Arya SP, Kishtawal CM, Shepherd M, Chen F, Wolfe B (2011) Urban modification of thunderstorms: an observational storm climatology and model case study for the Indianapolis urban region. J Appl Meteorol Climatol 50(5):1129–1144
Nugroho B, Hutchins N, Monty J (2013) Large-scale spanwise periodicity in a turbulent boundary layer induced by highly ordered and directional surface roughness. Int J Heat Fluid Flow 41:90–102. https://doi.org/10.1016/j.ijheatfluidflow.2013.04.003
Pardyjak ER, Stoll R (2017) Improving measurement technology for the design of sustainable cities. Meas Sci Technol 28(9):092,001
Patton EG, Shaw RH, Judd MJ, Raupach MR (1998) Large-eddy simulation of windbreak flow. Boundary-Layer Meteorol 87(2):275–307
Patton EG, Sullivan PP, Moeng CH (2005) The influence of idealized heterogeneity on wet and dry planetary boundary layers coupled to the land surface. J Atmos Sci 62(7):2078–2097
Patton EG, Sullivan PP, Shaw RH, Finnigan JJ, Weil JC (2016) Atmospheric stability influences on coupled boundary layer and canopy turbulence. J Atmos Sci 73(4):1621–1647
Peskin CS (1972) Flow patterns around heart valves: a numerical method. J Comp Phys 10(2):252–271. https://doi.org/10.1016/0021-9991(72)90065-4
Philips D, Rossi R, Iaccarino G (2013) Large-eddy simulation of passive scalar dispersion in an urban-like canopy. J Fluid Mech 723:404–428

Pino D, Jonker HJ, De Arellano JVG, Dosio A (2006) Role of shear and the inversion strength during sunset turbulence over land: characteristic length scales. Boundary-Layer Meteorol 121(3):537–556
Piomelli U, Balaras E (2002) Wall-layer models for large-eddy simulation. Annu Rev Fluid Mech 34:349–374
Piomelli U, Cabot WH, Moin P, Lee S (1991) Subgrid-scale backscatter in turbulent and transitional flows. Phys Fluids A 3(7):1766–1771. https://doi.org/10.1063/1.857956
Pope S (2000) Turbulent flows. Cambridge University Press, Cambridge
Pope SB (2004) Ten questions concerning the large-eddy simulation of turbulent flows. New J Phys 6:35–35. https://doi.org/10.1088/1367-2630/6/1/035
Porté-Agel F (2004) A scale-dependent dynamic model for scalar transport in large-eddy simulations of the atmospheric boundary layer. Boundary-Layer Meteorol 112(1):81–105. https://doi.org/10.1023/B:BOUN.0000020353.03398.20
Porté-Agel F, Meneveau C, Parlange MB (2000) A scale-dependent dynamic model for large-eddy simulation: application to a neutral atmospheric boundary layer. J Fluid Mech 415:261–284. https://doi.org/10.1017/S0022112000008776
Prandtl L (1925) 7. bericht über untersuchungen zur ausgebildeten turbulenz. ZAMM J Appl Math Mech Z Angew Math Mech 5(2):136–139. https://doi.org/10.1002/zamm.19250050212
Raasch S, Harbusch G (2001) An analysis of secondary circulations and their effects caused by small-scale surface inhomogeneities using large-eddy simulation. Boundary-Layer Meteorol 101(1):31–59
Raasch S, Schröter M (2001) PALM—a large-eddy simulation model performing on massively parallel computers. Meteorol Z 10(5):363–372
Rai RK, Berg LK, Kosović B, Haupt SE, Mirocha JD, Ennis BL, Draxl C (2019) Evaluation of the impact of horizontal grid spacing in terra incognita on coupled mesoscale-microscale simulations using the WRF framework. Mon Weather Rev 147(3):1007–1027
Randall DA, Shao Q, Moeng CH (1992) A second-order bulk boundary-layer model. J Atmos Sci 49(20):1903–1923
Raupach M (1992) Drag and drag partition on rough surfaces. Boundary-Layer Meteorol 60(4):375–395
Raupach M, Finnigan J, Brunet Y (1996) Coherent eddies and turbulence in vegetation canopies: the mixing-layer analogy. In: Boundary-layer meteorology 25th anniversary volume, 1970–1995. Springer, pp 351–382
Richardson H, Basu S, Holtslag A (2013) Improving stable boundary-layer height estimation using a stability-dependent critical bulk Richardson number. Boundary-Layer Meteorol 148(1):93–109
Sadique J, Yang XI, Meneveau C, Mittal R (2017) Aerodynamic properties of rough surfaces with high aspect-ratio roughness elements: effect of aspect ratio and arrangements. Boundary-Layer Meteorol 163(2):203–224
Sagaut P (2006) Large eddy simulation for incompressible flows: an introduction, 3rd edn. Springer, Berlin
Saiki EM, Moeng CH, Sullivan PP (2000) Large-eddy simulation of the stably stratified planetary boundary layer. Boundary-Layer Meteorol 95(1):1–30
Salesky ST, Anderson W (2018) Buoyancy effects on large-scale motions in convective atmospheric boundary layers: implications for modulation of near-wall processes. J Fluid Mech 856:135–168
Salesky ST, Chamecki M, Bou-Zeid E (2017) On the nature of the transition between roll and cellular organization in the convective boundary layer. Boundary-Layer Meteorol 163(1):41–68
Sandström U, Van den Besselaar P (2018) Funding, evaluation, and the performance of national research systems. J Informetr 12(1):365–384
Santos JM, Reis N, Castro I, Goulart EV, Xie ZT (2019) Using large-eddy simulation and wind-tunnel data to investigate peak-to-mean concentration ratios in an urban environment. Boundary-Layer Meteorol 172(3):333–350
Schalkwijk J, Jonker HJ, Siebesma AP (2016) An investigation of the eddy-covariance flux imbalance in a year-long large-eddy simulation of the weather at Cabauw. Boundary-Layer Meteorol 160(1):17–39
Schmidt H, Schumann U (1989) Coherent structure of the convective boundary layer derived from large-eddy simulations. J Fluid Mech 200:511–562
Schumann U (1975) Subgrid scale model for finite difference simulations of turbulent flows in plane channels and annuli. J Comp Phys 18(4):376–404. https://doi.org/10.1016/0021-9991(75)90093-5
Shao Y, Liu S, Schween JH, Crewell S (2013) Large-eddy atmosphere-land-surface modelling over heterogeneous surfaces: model development and comparison with measurements. Boundary-Layer Meteorol 148(2):333–356
Shaw RH, Patton EG (2003) Canopy element influences on resolved-and subgrid-scale energy within a large-eddy simulation. Agric For Meteor 115(1–2):5–17
Shaw RH, Schumann U (1992) Large-eddy simulation of turbulent flow above and within a forest. Boundary-Layer Meteorol 61(1–2):47–64

Shen S, Leclerc MY (1995) How large must surface inhomogeneities be before they influence the convective boundary layer structure? A case study. Q J R Meteorol Soc 121(526):1209–1228
Shepherd MJ (2005) A review of current investigations of urban-induced rainfall and recommendations for the future. Earth Interact 9(12):1–27
Shin HH, Dudhia J (2016) Evaluation of PBL parameterizations in WRF at subkilometer grid spacings: turbulence statistics in the dry convective boundary layer. Mon Weather Rev 144(3):1161–1177. https://doi.org/10.1175/MWR-D-15-0208.1
Shin HH, Hong SY (2015) Representation of the subgrid-scale turbulent transport in convective boundary layers at gray-zone resolutions. Mon Weather Rev 143(1):250–271. https://doi.org/10.1175/MWR-D-14-00116.1
Siebesma AP, Soares PM, Teixeira J (2007) A combined eddy-diffusivity mass-flux approach for the convective boundary layer. J Atmos Sci 64(4):1230–1248
Smagorinsky J (1963) General circulation experiments with the primitive equations. Mon Weather Rev 91:99–164. https://doi.org/10.1175/1520-0493(1963)091<0099:gcewtp>2.3.co;2
Sorbjan Z (1997) Decay of convective turbulence revisited. Boundary-Layer Meteorol 82(3):503–517
Sorbjan Z (2004) Large-eddy simulations of the baroclinic mixed layer. Boundary-Layer Meteorol 112(1):57–80
Sorbjan Z (2007) A numerical study of daily transitions in the convective boundary layer. Boundary-Layer Meteorol 123(3):365–383
Steeneveld G, Van de Wiel B, Holtslag A (2007) Diagnostic equations for the stable boundary layer height: evaluation and dimensional analysis. J Appl Meteorol Climatol 46(2):212–225
Stevens B, Moeng CH, Ackerman AS, Bretherton CS, Chlond A, de Roode S, Edwards J, Golaz JC, Jiang H, Khairoutdinov M, Kirkpatrick MP, Lewellen DC, Lock A, Müller F, Stevens DE, Whelan E, Zhu P (2005) Evaluation of large-eddy simulations via observations of nocturnal marine stratocumulus. Mon Weather Rev 133(6):1443–1462. https://doi.org/10.1175/MWR2930.1
Stoll R, Porté-Agel F (2006a) Effect of roughness on surface boundary conditions for large-eddy simulation. Boundary-Layer Meteorol 118(1):169–187
Stoll R, Porté-Agel F (2008) Large-eddy simulation of the stable atmospheric boundary layer using dynamic models with different averaging schemes. Boundary-Layer Meteorol 126(1):1–28
Stoll R, Porté-Agel F (2006b) Dynamic subgrid-scale models for momentum and scalar fluxes in large-eddy simulations of neutrally stratified atmospheric boundary layers over heterogeneous terrain. Water Resour Res 42(1):1–18. https://doi.org/10.1029/2005WR003989
Su HB, Shaw RH, Paw KT, Moeng CH, Sullivan PP (1998) Turbulent statistics of neutrally stratified flow within and above a sparse forest from large-eddy simulation and field observations. Boundary-Layer Meteorol 88(3):363–397
Sullivan PP, Patton EG (2011) The effect of mesh resolution on convective boundary layer statistics and structures generated by large-eddy simulation. J Atmos Sci 68(10):2395–2415
Sullivan PP, McWilliams JC, Moeng CH (1994) A subgrid-scale model for large-eddy simulation of planetary boundary-layer flows. Boundary-Layer Meteorol 71(3):247–276
Sullivan PP, Moeng CH, Stevens B, Lenschow DH, Mayor SD (1998) Structure of the entrainment zone capping the convective atmospheric boundary layer. J Atmos Sci 55(19):3042–3064
Sullivan PP, Weil JC, Patton EG, Jonker HJ, Mironov DV (2016) Turbulent winds and temperature fronts in large-eddy simulations of the stable atmospheric boundary layer. J Atmos Sci 73(4):1815–1840
Sun J, Lenschow D, Burns S, Banta RM, Newsom R, Coulter R, Nappo CJ, Frasier S, Ince T, Balsley BB (2004) Atmospheric disturbances that generate intermittent turbulence in nocturnal boundary layers. Boundary-Layer Meteorol 110(2):255–279
Svensson G, Holtslag AA (2009) Analysis of model results for the turning of the wind and related momentum fluxes in the stable boundary layer. Boundary-Layer Meteorol 132(2):261–277
Teixeira J, Stevens B, Bretherton C, Cederwall R, Doyle JD, Golaz JC, Holtslag AA, Klein S, Lundquist JK, Randall DA et al (2008) Parameterization of the atmospheric boundary layer: a view from just above the inversion. Bull Am Meteorol Soc 89(4):453–458
Tennekes H, Lumley J (1972) A first course in turbulence. MIT Press, Cambridge
Tomas J, Pourquie M, Jonker H (2016) Stable stratification effects on flow and pollutant dispersion in boundary layers entering a generic urban environment. Boundary-Layer Meteorol 159(2):221–239
Tseng YH, Meneveau C, Parlange MB (2006) Modeling flow around bluff bodies and predicting urban dispersion using large eddy simulation. Environ Sci Technol 40(8):2653–2662
van der Linden SJ, Edwards JM, van Heerwaarden CC, Vignon E, Genthon C, Petenko I, Baas P, Jonker HJ, van de Wiel BJ (2019) Large-eddy simulations of the steady wintertime antarctic boundary layer. Boundary-Layer Meteorol 173(2):165–192
Voller VR, Porté-Agel F (2002) Moore's law and numerical modeling. J Comp Phys 179(2):698–703

Walko RL, Cotton WR, Pielke RA (1992) Large-eddy simulations of the effects of hilly terrain on the convective boundary layer. Boundary-Layer Meteorol 58(1–2):133–150. https://doi.org/10.1007/BF00120755
Walton A, Cheng A (2002) Large-eddy simulation of pollution dispersion in an urban street canyon-part ii: idealised canyon simulation. Atmos Environ 36(22):3615–3627
Watanabe T (2004) Large-eddy simulation of coherent turbulence structures associated with scalar ramps over plant canopies. Boundary-Layer Meteorol 112(2):307–341
Willingham D, Anderson W, Christensen KT, Barros J (2013) Turbulent boundary layer flow over transverse aerodynamic roughness transitions: induced mixing and flow characterization. Phys Fluids 26(025):111-1–111-16
Wilson J (1988) A second-order closure model for flow through vegetation. Boundary-Layer Meteorol 42(4):371–392
Wong VC, Lilly DK (1994) A comparison of two dynamic subgrid closure methods for turbulent thermal convection. Phys Fluids 6(2):1016–1023. https://doi.org/10.1063/1.868335
Wood D (1981) The growth of the internal layer following a step change in surface roughness. Report TN—FM 57, Department of Mechanical Engineering, Universty of Newcastle, Australia
Wyngaard J (2004) Toward numerical modeling in the terra incognita. J Atmos Sci 61:1816–1826
Wyngaard J (2010) Turbulence in the atmosphere. Cambridge University Press, Cambridge
Wyngaard JC, Brost RA (1984) Top-down and bottom-up diffusion of a scalar in the convective boundary layer. J Atmos Sci 41(1):102–112
Wyngaard JC, Weil JC (1991) Transport asymmetry in skewed turbulence. Phys Fluids A 3(1):155–162
Xie Z, Castro IP (2006) LES and RANS for turbulent flow over arrays of wall-mounted obstacles. Flow Turbul Combust 76(3):291
Xie ZT (2011) Modelling street-scale flow and dispersion in realistic winds–towards coupling with mesoscale meteorological models. Boundary-Layer Meteorol 141(1):53–75
Xie ZT, Castro IP (2009) Large-eddy simulation for flow and dispersion in urban streets. Atmos Environ 43(13):2174–2185
Yaghoobian N, Kleissl J et al (2014) An improved three-dimensional simulation of the diurnally varying street-canyon flow. Boundary-Layer Meteorol 153(2):251–276
Yamaguchi T, Randall DA (2012) Cooling of entrained parcels in a large-eddy simulation. J Atmos Sci 69(3):1118–1136
Yan C, Huang WX, Miao SG, Cui GX, Zhang ZS (2017) Large-eddy simulation of flow over a vegetation-like canopy modelled as arrays of bluff-body elements. Boundary-Layer Meteorol 165(2):233–249
Yang D, Shen L (2010) Direct-simulation-based study of turbulent flow over various waving boundaries. J Fluid Mech 650:131–180
Yang J, Anderson W (2017) Numerical study of turbulent channel flow over surfaces with variable spanwise heterogeneities: topographically-driven secondary flows affect outer-layer similarity of turbulent length scales. Flow Turbul Combust 100(1):1–17. https://doi.org/10.1007/s10494-017-9839-5
Yang X, Sadique J, Mittal R, Meneveau C (2015) Integral wall model for large eddy simulations of wall-bounded turbulent flows. Phys Fluids 27(2):025,112
Yue W, Parlange MB, Meneveau C, Zhu W, Van Hout R, Katz J (2007) Large-eddy simulation of plant canopy flows using plant-scale representation. Boundary-Layer Meteorol 124(2):183–203
Zhang R, Wang G, Guo S, Zamora ML, Ying Q, Lin Y, Wang W, Hu M, Wang Y (2015) Formation of urban fine particulate matter. Chem Rev 115(10):3803–3855
Zhu X, Iungo GV, Leonardi S, Anderson W (2017) Parametric study of urban-like topographic statistical moments relevant to a priori modelling of bulk aerodynamic parameters. Boundary-Layer Meteorol 162(2):231–253